Magnetische Hysterese

Physikalisches Institut
Fachbereich Physik
Johann Wolfgang Goethe-Universität
Frankfurt am Main

NEU!

Magnetische Hysterese

Zur Vorbereitung

Befassen Sie sich anhand der Literaturmappe und der dort angegebenen weiterführenden Literatur mit den folgenden Punkten:

- Phänomenologie der ferromagnetischen Hysterese
- Eigenschaften bistabiler Systeme
- Beiträge zur (freien) Energie des Ferromagneten im Magnetfeld
- Stoner-Wohlfahrt-Modell zur Ableitung der magnetischen Hysterese eines Ferromagneten (kohärente Domänenrotation, Astroid)
- Phänomenologie des magneto-optischen Kerr-Effekts (MOKE)
- Grundlagen des Mikromagnetismus (Landau-Lifshitz-Gilbert-Gleichung)

Durchführung :

1) Messen Sie die magnetische Hysterese einer Cobalt-Schicht (ca. 100nm dick) in polarer MOKE-Geometrie.
2) Messen Sie die magnetische Hysterese eines Cobalt-Platin-Multilagensystems in polarer MOKE-Geometrie.
3) Bestimmen Sie jeweils die „Koerzitivfeldstärke" (Angabe des entsprechenden angelegten Stroms, da nicht kalibriert) und die Remanenz (bezogen auf die Sättigungsmagnetisierung) in den erhaltenen Hystereseschleifen.
   Bestimmen Sie auf die selbe Art Koerzitivfeldstärke" und Remanenz bei der zusätzlichen Schleife einer sehr dünnen Cobalt-Schicht.
4) Untersuchen Sie das Verhalten eines mikroskopischen, ferromagnetischen Partikels bei einer Ummagnetisierung anhand der numerischen Lösung der entsprechenden mikromagnetischen Gleichung (zusammen mit dem Betreuer; Simulationsprogramm zur Verfügung gestellt).

Zusatzaufgabe für Protokoll :

Diskutieren Sie die an den Cobalt-Schichten und dem Multilagensystem gemessenen Hysteresen bezüglich der Anisotropie ihrer Magnetisierung. Welches sind die leichten bzw. schweren Achsen?

Versuchsaufbau

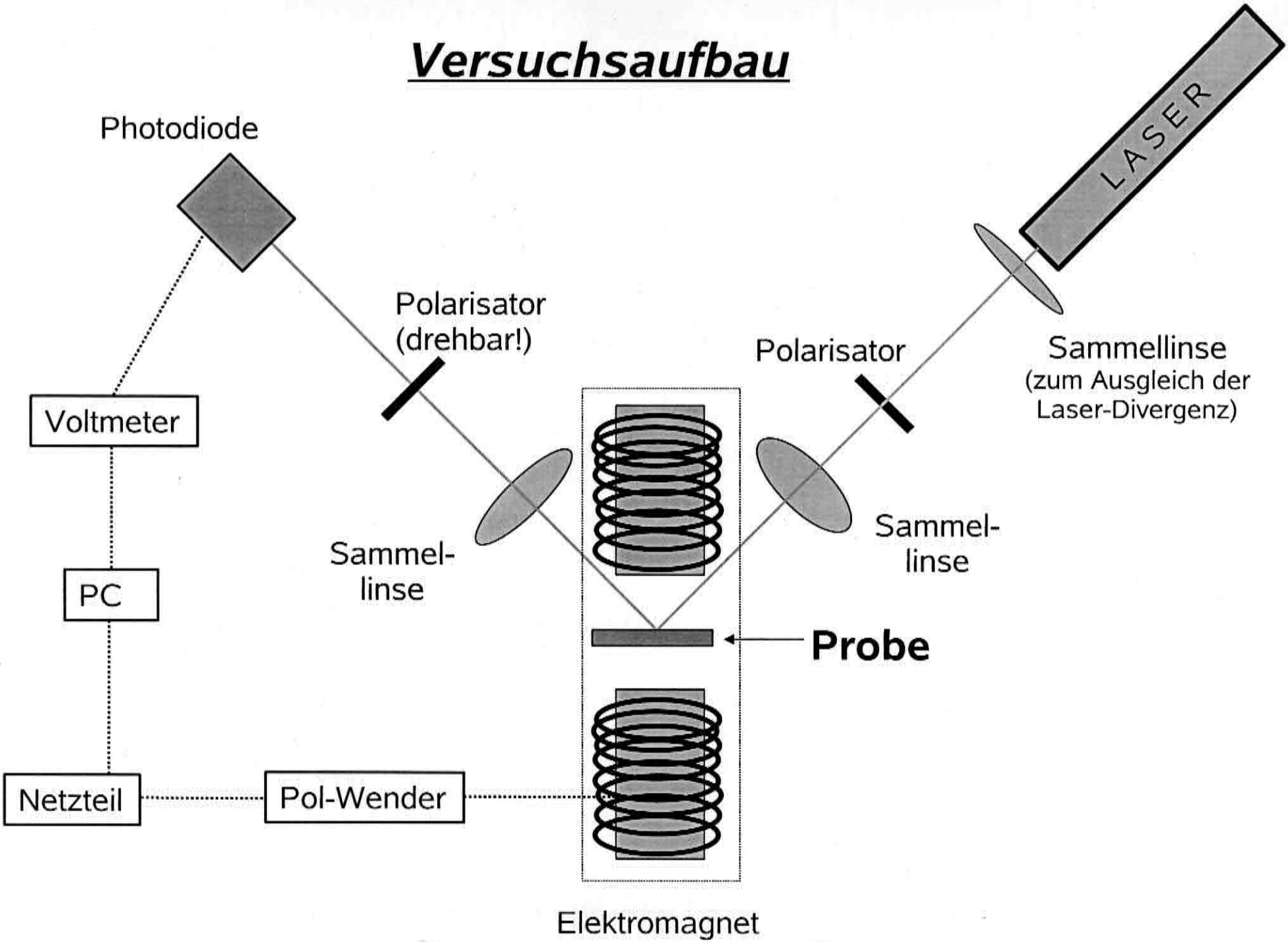

Magnetic Hysteresis

Hysteresis is at the heart of the behavior of magnetic materials. All applications, from electric motors to transformers and permanent magnets, from various types of electronic devices to magnetic recording, rely heavily on particular aspects of hysteresis. The variety of working conditions involved brings to light the fascinating richness of phenomena that may arise and drive the behavior of different materials. One soon realizes that naïve approaches, based on some empirical classification of material properties and on the use of limited phenomenological models developed on purpose, are largely inadequate for gaining convincing insight into the origin of the phenomena observed, or some significant power to predict them under various conditions. On the other hand, strong interest in hysteresis is not just the result of technological pressure. The comprehension of the physical mechanisms responsible for hysteresis and the development of adequate mathematical tools to describe it have attracted the attention of theoretical physicists and mathematicians for years. It is a beautiful example of a physical and mathematical problem of intriguing elegance and challenging complexity that is at the same time the source of pervading technological progress. Nobody can remain indifferent when considering the long but firm interdisciplinary chain that ties spin models of ferromagnetism to engineering applications of magnetic components.

The purpose of this chapter is to give an introductory overview of some general aspects of hysteresis, as they are observed in magnetic materials, and to make the reader acquainted with units, terms, and concepts frequently used in subsequent chapters. We illustrate some properties of hysteresis loops and their fundamental connection with magnetic domains. We discuss *rate-independent hysteresis, rate-dependent effects* (like eddy-current damping in metals), and *thermal relaxation* as the three fundamental classes of phenomena that may affect the behavior of a particular system. The presentation emphasizes qualitative aspects of general relevance, with little or no quantitative analysis. Frequent reference is made

to subsequent chapters, where the same subjects will be discussed in greater detail.

1.1 HYSTERESIS LOOPS

If we were asked to mention the experimental fact giving the most distinctive fingerprint of ferromagnetism, then, depending on our scientific background, we would probably propose either the existence of the *Curie point* or the observation of *hysteresis loops*, examples of which are shown in Fig. 1.1. Loops like these are obtained by applying to the specimen a cyclic magnetic field H and by recording the ensuing change of the magnetization M or of the magnetic induction B along the field direction. $\mathbf{M}$ measures the average magnetic moment per unit volume in the material and characterizes its magnetic state. In this book, we shall employ the *SI system of units*,[1] in which the magnetization, $\mathbf{M}$, and the magnetic field, $\mathbf{H}$, are measured in ampères per meter [Am^{-1}], whereas the magnetic induction, $\mathbf{B}$, and the magnetic polarization, $\mathbf{I} = \mu_0\mathbf{M}$, are measured in teslas [T]. $\mu_0 = 4\pi\,10^{-7}$ H m^{-1} is the permeability of the vacuum.

1.1.1 Hysteresis loops and magnetic domains

Hysteresis loops may take a variety of different forms and one would like to comprehend what are the basic physical mechanisms governing the observed phenomenology. We shall see that many interesting and highly nontrivial aspects contribute to the picture, and we shall have to go through several chapters of this book before attempting some convincing interpretation. Let us summarize here, as a simplified, introductory approach, the generally accepted view of the problem. A magnetic material can be imagined as an assembly of permanent magnetic moments $\mathbf{m}_i$, of quantum-mechanical origin. As an example, iron carries magnetic moments of $2.2\mu_B$ per atom, where the Bohr magneton $\mu_B = hq_e/4\pi m_e \cong 9.27\,10^{-24}$ A m^2 (h is Planck's constant, q_e and m_e are the electron charge and mass) is the natural atomic unit of magnetic moments. The simplest situation one may imagine is the one realized in an *ideal paramagnet*. This is a system where the individual $\mathbf{m}_i$ vectors do not interact with each other, but are independently shaken by thermal agitation. As a consequence, they take random orientations in space, which gives zero net magnetization in any macroscopic piece of material. However, a nonzero magnetization

[1] See Appendix A for more details on units.

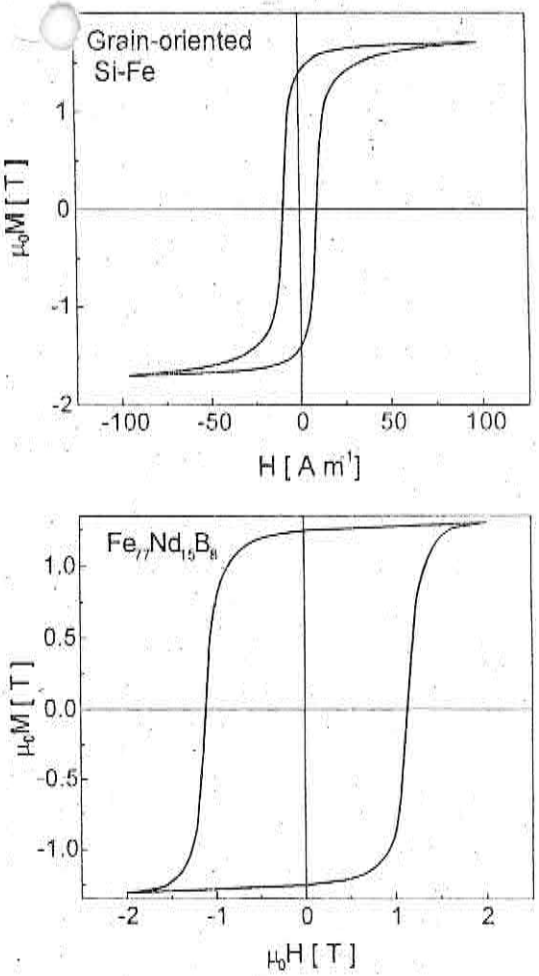

FIGURE 1.1. Hysteresis loops. Top: Grain-oriented 3 wt% Si-Fe alloy of the type used in transformer cores. Bottom: Sintered aligned $Fe_{77}Nd_{15}B_8$ permanent magnet (after Ref. 1.1). Loop widths differ by a factor of the order of 10^5.

can be induced by an external field $\mathbf{H}_a$. The potential energy of a single moment in the field is equal to $-\mu_0\mathbf{m}_i\cdot\mathbf{H}_a$. This energy term favors the alignment of the moments along the field direction. Conversely, the tendency of thermal agitation is just to destroy any order possibly present. An appreciable net magnetization component along the field is obtained when the field energy is at least comparable in order of magnitude to the thermal energy, which means that $\mu_0\mu_B H_a \sim k_B T$. At room temperature,

this would take place for fields $H_a \sim k_B T/\mu_0\mu_B \sim 3\ 10^8$ A/m, which is about 10^6 times the order of magnitude of the fields involved in the upper loop of Fig. 1.1. It is evident that fields of the order of $10 - 10^2$ Am^{-1} should be absolutely insufficient to overcome thermal agitation and produce any appreciable magnetization.

In 1907, Weiss suggested that *ferromagnetic materials* could exhibit a large spontaneous magnetization even at low fields because the elementary magnetic moments were by no means independent, as assumed in the previous picture of a paramagnet, but were strongly coupled by an internal field proportional to the magnetization itself, $H_W \propto M$, which he termed *molecular field*. The molecular field introduces a positive feedback mechanism, because the presence of a net magnetization produces a non-zero molecular field, which in turn acts on all moments trying to further align them. The result is that, below a critical temperature, the *Curie temperature* T_c, the magnetic moments spontaneously attain long-range order and the material acquires a substantial *spontaneous magnetization* M_s. The knowledge of the experimental value of T_c permits one to estimate the order of magnitude of H_W, because at the Curie point one expects $\mu_0\mu_B H_W \sim k_B T_c$. In the case of iron, where $T_c \sim 10^3$ K, one finds $H_W \sim k_B T_c/\mu_0\mu_B \sim 10^9$ Am^{-1}. Well below T_c, the moments are nearly perfectly aligned. In iron, at room temperature, this gives a spontaneous magnetization of the order of 2 T, which is the order of magnitude recorded in Fig. 1.1.

The molecular field hypothesis explains the main aspects of the temperature dependence of the spontaneous magnetization, but it raises other conceptual difficulties. If there exists an internal field as enormous as the estimate of 10^9 Am^{-1} seems to indicate, then one would expect to find ferromagnetic materials spontaneously magnetized to saturation under all circumstances. Thus how can a hysteresis loop exist at all? It would seem impossible that fields of the order of 10 Am^{-1} can reduce to zero the magnetization of a ferromagnet, if they are confronted with internal fields of the order of 10^9 Am^{-1}. Weiss proposed to resolve this difficulty by postulating that a ferromagnetic material is subdivided into regions, called *magnetic domains*. In each domain, the degree of magnetic moment alignment is dictated by the molecular field, but the orientation of the spontaneous magnetization can vary from domain to domain. As a consequence, when the magnetization is averaged over volumes large enough to contain many domains, one obtains values mainly determined by the relative orientation and volume of domains. The result can be very different from the spontaneous magnetization, and even close to zero.

In a sense, the history of the comprehension of magnetic materials in the twentieth century has been, above all, the history of the elaboration of Weiss' ideas. It took many years before quantum mechanics could give some hint to the microscopic interpretation of the molecular field. It took even longer before the importance of the concept of magnetic domain could be fully appreciated and exploited. In fact, we shall see that magnetic domains are the result of the complex and delicate balance of several competing energy terms, a balance by no means trivial to treat theoretically. However, these difficulties did not prevent domains from acquiring the status of real objects of the physical world, when direct domain observation became a reality. Nowadays, a number of techniques based on magneto-optics, electron microscopy, and other principles permit one to produce magnetic domain images of striking evidence and beauty that have become the common way to characterize magnetic materials (see Fig. 1.2).

The variety of observed hysteresis loop shapes is the direct consequence of the variety of possible magnetic domain structures. Magnetic domains result from the balance of several competing energy terms: *exchange energy* (strictly related to the molecular field and discussed in Chapter 5), which favors uniform magnetization configurations; *magnetocrystalline anisotropy* (due to interactions of the magnetization with the hosting lattice, also discussed in Chapter 5), which favors the orientation of the magnetization vector along certain preferred directions; and *magnetostatic energy* (discussed in chapters 3 and 4), which on the contrary favors magnetization configurations giving a null average magnetic moment. A domain structure like the one shown in Fig. 1.2 represents the compromise by which the system tries to satisfy all these competing requirements. In addition to these internal mechanisms, the magnetization is coupled to the external field by the energy $-\mu_0\mathbf{M}\cdot\mathbf{H}_a$, which favors domains magnetized in the direction of the applied field. When $\mathbf{H}_a$ varies in time, the energy balance is altered and rearrangements of the domain structure take place, mainly through the motion of the interface layers, known as *domain walls*, separating adjacent domains. The domains with magnetization approximately pointing in the direction of the applied field are energetically favored and expand at the expenses of surrounding domains, which shrink and eventually disappear (Fig. 1.3). At high fields, the material is everywhere magnetized along the applied field direction and we practically have one big domain occupying the whole specimen. Here is where the average magnetization of the specimen becomes close to the spontaneous magnetization. When the field is reversed, domains of reversed magnetization are formed, which progressively increase in size through domain wall motion, until a single domain of reversed magnetization is formed.

This description gives a good qualitative interpretation of the mechanisms behind the hysteresis loop of many magnetic materials. Nonetheless, it is oversimplified in many respects, as will become clear in Part III.

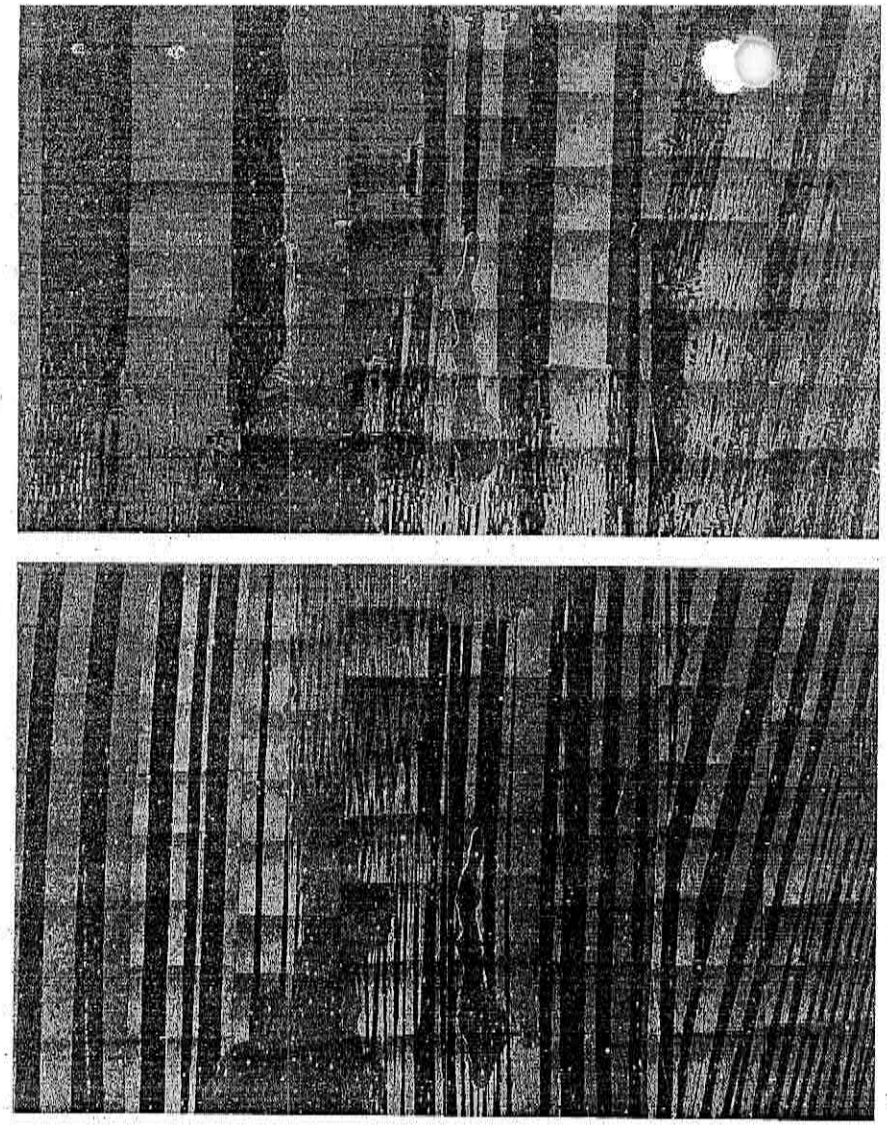

FIGURE 1.2. Magnetic domain structure in a lamination of grain-oriented 3 wt% Si-Fe alloy of the type considered in Fig. 1.1, observed by the Kerr-effect method. The magnetization is in the plane of the figure, and points along opposite directions (up and down) in white and black domains. The two pictures refer to the same portion of lamination, under different stress conditions. Top: Unstressed. Bottom: Subjected to a tensile stress along the vertical direction of 20 MPa. The regular horizontal striations result from the fact that the picture is made up of many photographs collected together and have no particular meaning. The horizontal dimension of the observed region is approximately 1.5 cm: (After Ref. 1.2)

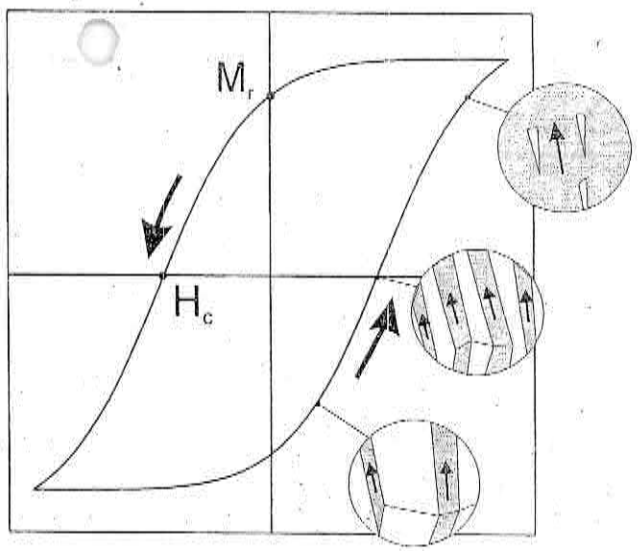

FIGURE 1.3. Schematic representation of hysteresis loop and ensuing evolution of magnetic domains.

The domain approach is in the end an approximation that can sometimes become inadequate. There may be cases where the clear-cut identification of well-separated domains becomes ambiguous and questionable. In other cases, domains may simply not exist at all. In Part III and IV, a detailed discussion of the cases where the domain picture might fail will be given.

1.1.2 Hysteresis loop properties

Hysteresis loops may take many different shapes and it is important to list a few parameters that give some prime characterization of loop properties. Two quantities of particular importance in this respect are the remanent magnetization or *remanence*, M_r, and the *coercive field*, H_c.

Remanence. This represents the magnetization obtained after applying a large field to the specimen and then removing it. It is the natural quantity expressing the fact that a ferromagnet can be spontaneously magnetized, even in the absence of external actions. The order of magnitude of M_r is that of the spontaneous magnetization M_s, but various geometrical or structural features may contribute to decreasing M_r well below M_s.

Coerçive field. This is the field needed to bring the magneti[illegible] from the remanent value to zero. The coercive field measures the [illegible] of magnitude of the fields that must be applied to a material in order to reverse its magnetization. Unlike remanence, the coercive field spans an astonishingly wide interval, from less than 1 Am^{-1} to more than 10^6 Am^{-1}. An example is given by the two loops shown in Fig. 1.1.

Materials can be classified according to the values taken by these parameters and others related to them. In particular, it is common to subdivide materials into *soft* and *hard* magnetic materials.

Soft magnetic materials. The term soft material is used to refer to materials that are easy to magnetize, destined to applications where a low coercive field is a prime requirement. The coercive field is of the order of 50–100 Am^{-1} in nonoriented Si-Fe alloys and low-carbon steels used in electric motors and other components, and decreases down to 10 Am^{-1} in grain-oriented Si-Fe alloys employed in transformer cores. This is also the typical coercivity value in Mn-Zn and Ni-Zn ferrites. Extremely soft materials can be obtained from nickel-based alloys with approximately 80% Ni and 20% Fe, generically known as permalloys. With the advent of the rapid solidification technology, it has become possible to produce amorphous alloys composed of about 80% transition metals (chiefly Fe and/or Co) and 20% metalloids (B, Si, C), and nanocrystalline alloys, with grains of dimensions in the nanometer range immersed in an amorphous matrix, which rival permalloys in softness. Under optimal conditions, permalloys and rapidly solidified alloys can exhibit coercive fields around or even below 1 Am^{-1}. An additional parameter of basic importance in the characterization of soft materials is the *power loss*, proportional to the area of the hysteresis loop. A low loss is one of the chief indicators used to monitor the quality of soft materials. What is important to control, in particular, is the increase of the hysteresis loop area with increasing magnetization frequency brought about by eddy current damping. This calls for a detailed study of dynamic hysteresis effects, along the lines discussed in this chapter (Section 1.3.1) and in Chapter 12.

Hard magnetic materials. Hard magnetic materials are devoted to applications where, contrary to soft materials, one wants the material to be a stable and permanent source of magnetic field, insensitive to external actions. The coercive field is of the order of 50–100 kAm^{-1} in alnico alloys, containing various proportions of Fe, Ni, Co, Al, and Cu. In hexagonal ferrites, which are iron oxides of the type $BaFe_{12}O_{19}$ or $SrFe_{12}O_{19}$, H_c can be around 300 kAm^{-1}, but it can exceed 1000 kAm^{-1} in rare-earth magnets of the Sm-Co or Nd-Fe-B type. More than coercivity, a parameter important in estimating th[illegible]rength of a hard magnet is the *maximum energy product*, discussed in S[illegible] 10.2.3, which gives a measure of the energy made available by the magnet for external work. A theoretical upper bound for energy products is given by $\mu_0 M_s^2/4$, where M_s is the spontaneous magnetization. With $\mu_0 M_s \sim 2$ T, like in iron, we obtain $\mu_0 M_s^2/4 \sim 800$ kJ m^{-3}. Typical values of energy products range from 30–50 kJ m^{-3} (in ferrites and alnicos) to 300 kJ m^{-3}.

Magnetic recording. Although this term does not identify a particular class of magnetic materials, it is important to mention it as a technological area where hysteresis is exploited at its uppermost possibilities. Medium-hard materials are employed to permanently store recorded information ($H_c \sim$ 20–30 kA m^{-1} in iron-oxide media for tape recording) and soft materials are used in the recording heads necessary to write, read, and erase the recording information.

A hysteresis loop can be represented in terms of $B(H)$ or of $M(H)$. The relation between magnetization and induction is $\mathbf{B} = \mu_0(\mathbf{H} + \mathbf{M})$. In a soft material, the fields involved in the hysteresis loop are much smaller than the corresponding magnetization values (see Fig. 1.1), so that, to a very good approximation, $\mathbf{B} \cong \mu_0\mathbf{M}$ and plotting $B(H)$ or $M(H)$ makes a tiny difference that can be safely neglected. Conversely, in hard materials $\mathbf{H}$ and $\mathbf{M}$ have comparable orders of magnitude, and the $B(H)$ loop is significantly different from the $M(H)$ one (Fig. 1.4). For example, there are two possible definitions for the coercive field, depending on whether one considers the point where the induction or the magnetization is reduced to zero. The $M(H)$ loop better reflects the intrinsic properties of the magnet, but the $B(H)$ loop gives a more useful description of the system behavior under working conditions. For instance, the maximum energy product previously mentioned is directly related to the $B(H)$ loop.

1.1.3 Difficulties in hysteresis loop interpretation

Hysteresis loops are so often presented and discussed that it is easy to forget the many difficulties hidden behind them. The point is that a hysteresis loop can hardly be interpreted as a property of the material considered, but it is rather the outcome of a number of steps, where the measurement method, the specimen geometry, and several other nontrivial assumptions have a role. For example, field and magnetization are vector quantities. Therefore, in principle, any representation of hysteresis loops should be given in vector terms. On the contrary, many experiments and theoretical interpretations are based on a scalar representation, where the magnetization component along the field is given as a function of the

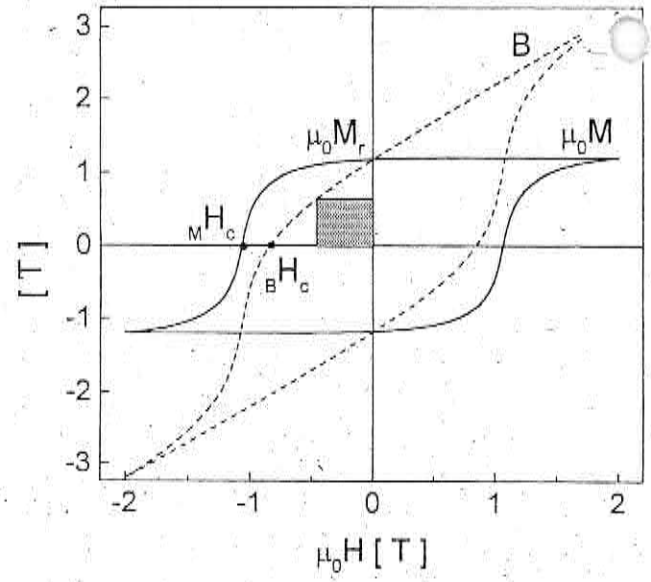

FIGURE 1.4. Difference between $B(H)$ and $M(H)$ hysteresis loops in hard magnets. The shaded rectangular area represents the energy product associated with a given point of the $B(H)$ curve.

field intensity. This scalar description is of tempting clarity and simplicity, and it is quite convenient in all cases where some kind of anisotropy identifies a privileged direction in the problem, but it is always to some extent incomplete, because it says nothing about the behavior of the magnetization component perpendicular to the field.

There are many techniques to measure hysteresis loops and it is outside the scope of this book to discuss magnetic measurements. Let us just consider, as an example, the schematic arrangement shown in Fig. 1.5. A current I_p is passed through a primary coil in order to generate a magnetic field of intensity H_a, proportional to the current, along the ring. The presence of the field alters the magnetic state of the material, which results in a change of the magnetic induction **B** inside the ring. The voltage V_s induced in the secondary coil is proportional to the rate of change of the flux $\Phi = S\langle B\rangle$, where S is the area of the material cross-section linked to the coil, and $\langle B\rangle$ is the average induction component perpendicular to that cross-section. We suppose to deal with a soft material for which $\langle B\rangle \cong \mu_0\langle M\rangle$. The result of a measurement of this type is usually presented by plotting $\langle M\rangle$ as a function of H_a. Some comments are appropriate as

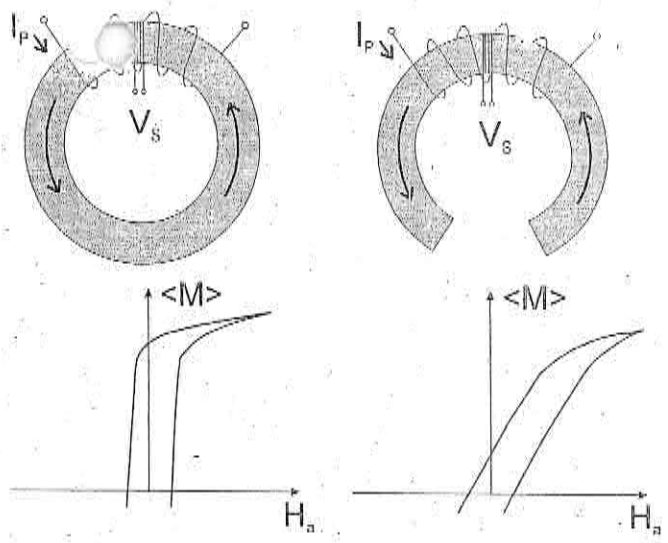

FIGURE 1.5. Schematic arrangement for hysteresis loop measurement. The shape of the loop measured on the same material is affected by the specimen geometry.

regards the role of both field and magnetization in the hysteresis loop thus obtained.

Applied field. H_a, as calculated from the primary current, is the magnetic field that would be present inside the primary coil if no magnetic material were there. When the same primary current is used to excite the material, the relation between fields and currents is changed by the presence of the material itself, and it is not at all obvious that we can use the field pertaining to empty space to characterize the situation where that space is filled with magnetized matter. In fact, when the same experiment on the same material is carried out for a different specimen geometry, like the horseshoe geometry shown to the right of Fig. 1.5, a completely different result is obtained. As discussed in Chapter 3, the difference derives from the fact that, for the same applied field H_a, the effective field H acting in the material is, in the case of the horseshoe geometry, $H = H_a - N\langle M\rangle$. The term $N\langle M\rangle$, proportional to the specimen magnetization, is the so-called *demagnetizing field*, and the *demagnetizing factor* N is determined by the specimen geometry. One can try corrections, where the effective field is obtained from H_a through some estimate of N, in order to derive what one would like to consider the "real" hysteresis loop of that material. Corrections of this kind are often not simple to carry out in practice. The mathematics and the physics of magnetostatic fields is

complicated enough, and analytic solutions are known only for a few special sample geometries. Extrapolation to more complicated situations introduces its own problems and approximations. The difficulty, however, is not just in having a reliable estimate of the demagnetizing field. The two situations shown in Fig. 1.5 are physically different and a direct correspondence between them might simply not exist at all. As an example, consider the loops of Fig. 1.6, measured on wires of the same soft amorphous material, for two different wire lengths. The long wire has a typical bistable behavior. The magnetization is abruptly reversed in one jump when H_a reaches a certain critical value. This bistable behavior is partly inhibited in the shorter wire by the presence of a larger demagnetizing field, which stops the magnetization jump on the way and gives rise to a qualitatively different loop.

Magnetization. As regards $\langle M \rangle$, we have mentioned the fact that $\langle M \rangle$ is the result of a space average over appropriate volumes of the specimen. The measured loop thus describes some macroscopic property of the whole specimen, rather than some local property of the material. Even though the $\langle \ldots \rangle$ brackets are seldom indicated explicitly, one should bear in mind that some space average is always involved. This point is of particular importance because one is often tempted to simplify the description of a given magnetic material by directly interpreting the loops of Fig. 1.1 as the constitutive law $M(H)$ describing the material response to magnetic fields. As discussed in the next section, this assumption is

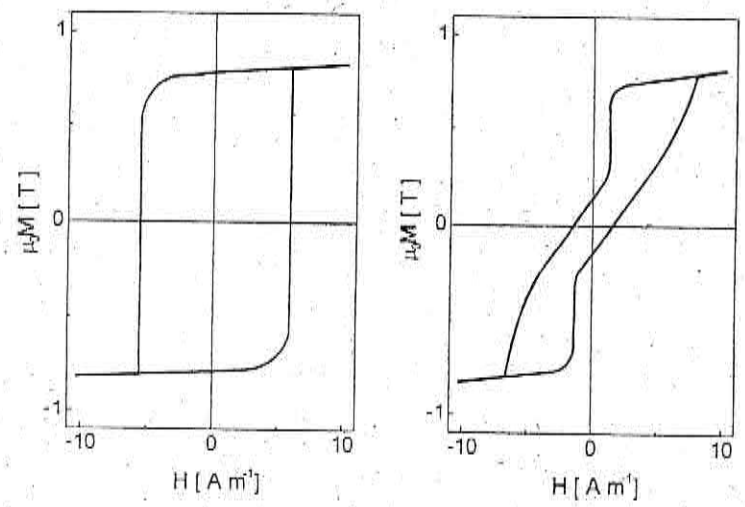

FIGURE 1.6. Hysteresis loops measured on $Fe_{77.5}Si_{7.5}B_{15}$ amorphous wires with different lengths l. Left: l = 13.1 cm. Right: l = 5.2 cm. (After Ref. 1.3)

certainly questionable in that a single hysteresis loop is by no means sufficient to give a complete representation of magnetic hysteresis. However, even if this difficulty were not there, assuming a direct link between the measured loop and the material response is of little physical meaning if it is not accompanied by some qualification concerning spatial scales. Let us reconsider our idealized picture of a magnetic material as an assembly of magnetic moments $\mathbf{m}_i$. Let us subdivide the material into small *elementary volumes* ΔV, where by small we mean that their extension must be small with respect to the distances over which significant variations of the material properties take place. On the other hand, we want ΔV to be large enough to contain many elementary moments, in order to justify a reliable use of statistic and thermodynamic methods to describe its properties. The magnetization $\mathbf{M}$, when averaged over ΔV, appears as a vector of fixed modulus, equal to the spontaneous magnetization M_s, but with variable orientation from point to point in space. At the ΔV scale, there is no uniquely defined material response, because the relationship between $\mathbf{M}$ and $\mathbf{H}$ will be in general different from point to point, as a consequence of the presence of magnetic domains and of structural disorder. For example, in cases where some preferred direction for $\mathbf{M}$ exists, like in Fig. 1.2, and the external field is applied along that direction, one may expect the local $\mathbf{M}$ component along the field to describe a nearly square loop, with $\mathbf{M}$ abruptly switching between opposite orientations at certain threshold field values, differing from point to point. If, starting from this local behavior, we could take the average of $\mathbf{M}$ and $\mathbf{H}$ over progressively larger volumes, we would see the $\mathbf{M}$-$\mathbf{H}$ relationship gradually changing from the elementary square loop just described to the macroscopic loop of Fig. 1.5.

The emergence of the macroscopic hysteresis behavior is intimately related to the existence of magnetic domains. It is only over scales larger than the domain size that the macroscopic hysteresis properties of a material become manifest. Notice that the scale of domains is not necessarily closer to the atomic scale than to the geometric scale of the specimen. In certain magnetic materials, like the one of Fig. 1.2, domain size can be in the range of millimeters, rather than of nanometers. This problem of the correct treatment of spatial scales is of pervading importance. Many properties that we shall address in the next chapters will be scale-dependent or will have significance only in a certain range of scales. On the other hand, in all cases where we are interested in the gross spatial features of a problem that take place on scales larger than the domain size, we can choose the elementary volumes ΔV larger than the domain size from the beginning. When adopting this low-resolution viewpoint,

the "local" magnetization vector is no longer a vector of fixed magnitude and variable orientation, as it is already the result of an average over many domains. On the contrary, in many cases it will appear as a vector of variable intensity, pointing along some privileged direction of the problem. On this scale, the material appears to be magnetically homogeneous and the idea of giving a constitutive law $M(H)$ describing the response of each elementary volume to magnetic fields becomes meaningful and fruitful.

The conclusion is that one must be extremely careful in associating a hysteresis loop with a given material, without specifying the experimental conditions, the geometry, the spatial scale we are interested in, not to say all those chemical and metallurgical aspects involved in material preparation. There exists nothing that we can straightforwardly call the "hysteresis loop of iron."

so high that appreciable field variations take place during individual Barkhausen jumps, then rate-independence no longer applies. The system no longer evolves through a sequence of spontaneous jumps but approaches a regime of forced dynamic evolution driven by the external field. This transition from rate-independent to rate-dependent hysteresis will be discussed in Section 2.3.

2.2 RATE-INDEPENDENT HYSTERESIS

In this section we discuss rate-independent hysteresis and energy dissipation, along the lines anticipated at the end of the preceding section. In principle, one should address the subject by considering a multidimensional energy landscape, with a complicated multivalley structure and nonlocal memory effects. Yet, this is too complex a problem to be a good starting point. We prefer to show how many of the phenomena in which we are interested are already present in the simple case of a *bistable system*, whose free energy is characterized by two minima only. This is a system with local memory, where, in addition, there are at most two metastable states available to the system. In spite of its simplicity, this case illustrates well several important aspects present under more general conditions. In addition, we shall see, especially in chapters 10, 13, and 14, that complicated situations can often be approximately described just in terms of the superposition of many elementary bistable contributions.

2.2.1 Bistable systems

Let us consider a system whose free energy is given by the expression[3]

$$f(x) = x^4 - 2ax^2 \tag{2.23}$$

where a is a positive constant. We use lowercase letters to indicate that the problem has been reduced to some convenient dimensionless form, in which all variables and parameters are dimensionless. $f(x)$ is shown in Fig. 2.4. It has two equal minima located at $x = \pm a^{1/2}$, and a maximum at $x = 0$. According to Eq. (2.18), the free energy under nonzero input h will be

$$g_L(x;h) = x^4 - 2ax^2 - hx \tag{2.24}$$

[3]The temperature dependence is not important for the subsequent considerations and will be understood in the rest of this section and throughout Section 2.3.

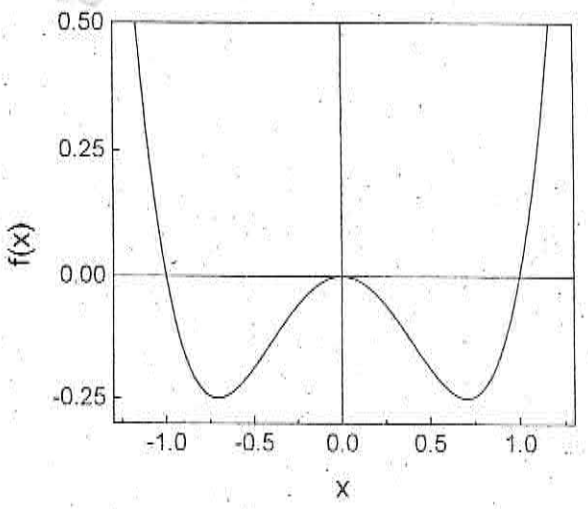

FIGURE 2.4. Free energy of bistable system described by Eq. (2.23), with $a = 0.5$. The energy minima are located at $x = \pm x_r = \pm a^{1/2}$.

The metastable states under the generic field h are determined by the condition $\partial g_L / \partial x = 0$, with $\partial^2 g_L / \partial x^2 > 0$, identifying local g_L minima. The qualitative behavior of $g_L(x;h)$ for various values of h is shown in Fig. 2.5. When h is large, the energy of interaction with the external field dominates and g_L exhibits only one minimum. When h increases from $-\infty$, at a certain field $-h_c$ to be determined later, a new energy minimum is formed. At $h = 0$ the two minima have the same energy. At $h = h_c$ the minimum initially occupied by the system becomes an inflection point:

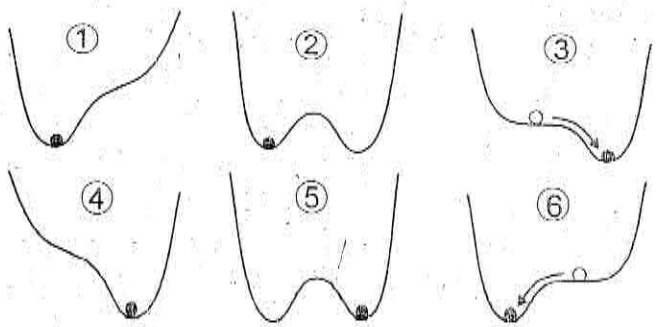

FIGURE 2.5. Sequence of energy profiles calculated from Eq. (2.24) under different external fields, showing genesis of Barkhausen jumps and hysteresis loop. The numbers refer to the field values indicated in Fig. 2.6.

the system is no longer stable and makes a spontaneous and irreversible Barkhausen jump to the lower energy state. Only one minimum is present for higher fields. A similar situation is found when the field is progressively decreased from $+\infty$, except for the fact that the Barkhausen jump will now take place at $h = -h_c$. We can represent the same situation by plotting the free energy gradient $\partial f/\partial x$ and by considering that, according to the equilibrium requirement $\partial g_L/\partial x = 0$, the condition $h = \partial f/\partial x$ must always be satisfied as the system evolves (Fig. 2.6). The $\partial f/\partial x$ profile can be decomposed into two stable branches, one for $x < -x_c$ and the other for $x > x_c$, where $\partial^2 f/\partial x^2 > 0$, and a central unstable branch where $\partial^2 f/\partial x^2 < 0$. The right stable branch is traversed when h decreases from $+\infty$ down to $h = -h_c$. At $h = -h_c$, $x = x_c$, the right branch ends and the system jumps to the point $h = -h_c$, $x = -x_f$ of the left branch. A similar description applies for increasing fields.

If we plot the state variable x as a function of the input field h, we obtain the hysteresis loop shown in Fig. 2.7. In spite of its simple structure, this loop already exhibits many of the features of the hysteresis loops actually observed in real systems. The two stable states existing at $h = 0$ are examples of remanent states. There the state variable takes the value $x = \pm x_r$, determined by the condition $\partial f/\partial x = 4x(x^2 - a) = 0$, which gives $x_r = \pm a^{1/2}$. The two instability points $h = h_c$, $x = -x_c$ and $h = -h_c$, $x = x_c$, where the Barkhausen jumps take place, are points where the two conditions, $\partial g_L/\partial x = 0$ and $\partial^2 g_L/\partial x^2 = 0$, must simultaneously hold, that is,

$$\begin{aligned} 4x^3 - 4ax - h &= 0 \\ 3x^2 - a &= 0 \end{aligned} \qquad (2.25)$$

The solution gives $h_c = 8(a/3)^{3/2}$, $x_c = (a/3)^{1/2}$. The final state $x = x_f > 0$ reached by the system after the Barkhausen jump at $h = h_c$ is also a solution of the equation $4x_f^3 - 4ax_f - h_c = 0$, with $3x_f^2 - a > 0$. One finds $x_f = 2(a/3)^{1/2}$.

In Section 2.1.2, we showed that the area of the hysteresis loop measures the amount of work dissipated as heat during each excitation cycle. This dissipation takes place in the Barkhausen jumps and is directly related to the g_L energy. Let us consider the shaded area ΔW shown in Fig. 2.6. By construction, this area is equal to the integral

$$\begin{aligned} \Delta W &= \int_{-x_c}^{x_f} \left[h_c - \frac{\partial f}{\partial x} \right] dx = -\int_{-x_c}^{x_f} \left[\frac{\partial g_L}{\partial x} \right]_{h = h_c} dx \\ &= g_L(-x_c; h_c) - g_L(x_f; h_c) \end{aligned} \qquad (2.26)$$

This is exactly the energy decrease occurring when the system makes the

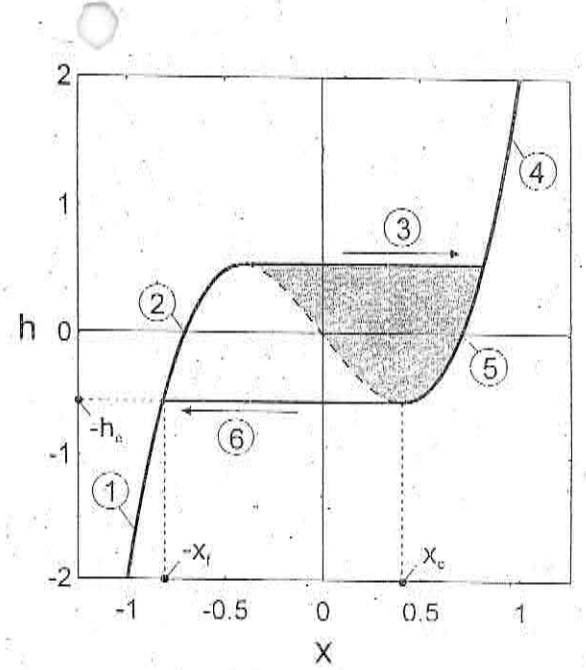

FIGURE 2.6. Equilibrium between thermodynamic forces in bistable system and genesis of hysteresis loop. The numbers refer to the energy profiles of Fig. 2.5.

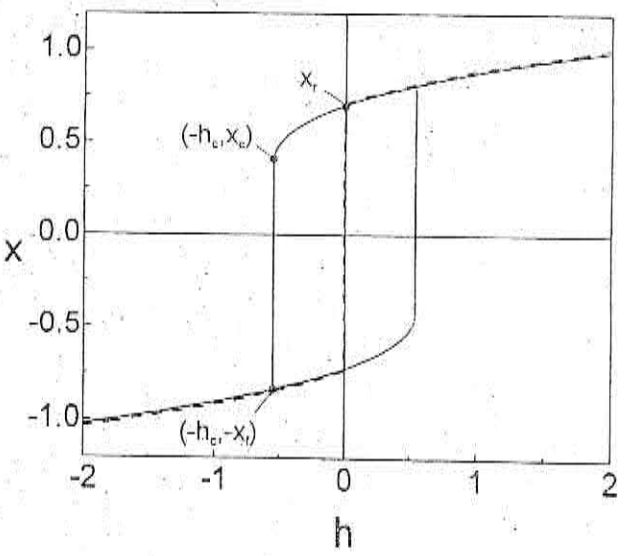

FIGURE 2.7. Solid line: Hysteresis loop of bistable system. Compare with Fig. 2.6. Broken line: Phase coexistence curve obtained by applying Maxwell convention.

Barkhausen jump (see Fig. 2.5). The system suddenly reduces its energy and transfers the energy difference as heat to the thermal bath. The same occurs in the jump taking place under a decreasing field. As shown by Fig. 2.6, the areas associated with the two jumps just sum up to give the total hysteresis loop area. This description makes clear the two steps through which the work performed by external sources is transformed into heat. Initially, the system gains energy from the external field as the minimum it occupies grows in energy and becomes less and less deep. Then, at the point where the minimum becomes an inflection point, the energy previously gained is quickly transferred to the thermal bath as the system jumps to lower energy, and the whole process can start again. Note also that the description is rate-independent, because we have assumed that the system always occupies one of the energy minima existing at the given field, whatever the field rate of change is. In particular, when we draw the two horizontal branches of Fig. 2.6 associated with the two Barkhausen jumps, we are implicitly assuming that the field does not change appreciably during the time needed by the system to make the jump. In Section 2.3, we will see how rate-dependent hysteresis naturally emerges when this assumption no longer holds.

2.2.3 Evolution rules and phase coexistence

Knowledge of the number and the nature of equilibrium points does not clarify which of these points will actually be occupied by the system. In principle, this would require some dynamic description of the system evolution, of the type discussed in Sections 2.3 and 2.4. A simpler approach, adopted in catastrophe theory, is to summarize such dynamic aspects through appropriate conventions. Two extreme cases are in particular considered.

Delay convention. The system remains in the equilibrium state initially occupied until this state is made unstable by the action of the control parameters.

Maxwell conventic The system always occupies the state where the potential is at its absol minimum.

The *delay convention* is exactly the one on which we have based our description of rate-independent hysteresis. The behavior illustrated by Fig. 2.5 can be rephrased in the frame of catastrophe theory as follows. The evolution of the system is represented by the horizontal line of Fig. 2.9. The points where the evolution line crosses the bifurcation set are the only points where Barkhausen jumps can take place. In this context, a Barkhausen jump is an event in which a small change in the control parameters entails a substantial change in the state variables. Any crossing of the bifurcation set will not necessary lead to a Barkhausen jump. For this to occur, the system must be in one of the equilibrium states disappearing at the crossing. With reference to the horizontal evolution line of Fig. 2.9, one can check that a Barkhausen jump occurs only when the evolution point exits the cusp region. In general, for a Barkhausen jump to occur, the system must enter the cusp region from one side (e.g., $h < 0$) and exit through the opposite one (e.g., $h > 0$).

The *Maxwell convention* can instead be interpreted as an approximate description of situations where the effect of thermal agitation is so important that the system rapidly relaxes to the state of minimum energy in times much shorter than the time scale over which the input exhibits significant variations. When the Maxwell convention is adopted, a new bifurcation set can be defined, known as the *Maxwell set*. This is the set of points in control space where the value of the potential at two or more minima becomes the same. The Maxwell set for the potential of Eq. (2.24) is described by the condition $h = 0$ and is represented by the broken line of Fig. 2.9. When the system reaches the Maxwell set, the state variable changes by a finite amount even under constant field. This is shown, for example, by the broken line of Fig. 2.7. This discontinuity is, however, perfectly reversible and entails no energy dissipation.

From the thermodynamic viewpoint, a free energy like the one shown in Fig. 2.4 points at the existence of two possible *phases* for the system, each corresponding to one of the two equivalent energy minima, $x = x_r$ and $x = -x_r$. One might wonder if there may be any possibility to have stable states where $x = 0$. As $x = 0$ is an energy maximum, no such state is possible if we look for spatially homogeneous states, where x has the same value at each point in space. However, if we are dealing with a spatially extended system and we are only interested in the mean value $\langle x \rangle$ of x over the whole volume of the system, we can realize the condition $\langle x \rangle = 0$ by a *phase mixture*, in which half of the volume is in the $x = x_r$ phase and half is in the $x = -x_r$ phase. By introducing the concept of

states not homogeneous in space, made up of *domains* where the system is in one or the other phase (see Fig. 2.10), we can actually generate states that continuously span the interval $-x_r \leq \langle x \rangle \leq +x_r$, by adjusting the relative volumes of the two phases. The free energy of the mixture is a simple linear combination of the energies of the two phases, if we can neglect the energy concentrated at the interfaces separating different domains. In this frame, the Maxwell set can be interpreted as the set where *phase coexistence* is realized. When the system moves along the vertical broken line of Fig. 2.7, both phases are present, and the system smoothly passes from the condition $\langle x \rangle = -x_r$ (whole system in the $x = -x_r$ phase) to the condition $\langle x \rangle = x_r$ (whole system in the $x = x_r$ phase) with no hysteresis, by adjusting the relative volume of domains.

Magnetic domains are at the heart of the behavior of magnetic materials. However, the free energy structure responsible for them is more complicated than the simple bistable one considered here, and requires a specific detailed analysis. This aspect will be addressed in Part III.

Magnetische Domänenmuster

Um die Gesamtenergie zu reduzieren, und weil die Streufelder langreichweitiger sind als die Austauschfelder, gibt es charakteristische Größen von Bereichen (Domänen), in denen die Magnetisierung fast homogen ist.

Zwischen solchen Domänen treten notwendigerweise Übergänge, sogenannte **Domänenwände** auf. Ihre Art wird durch Materialparameter, Dicke, etc. bestimmt.

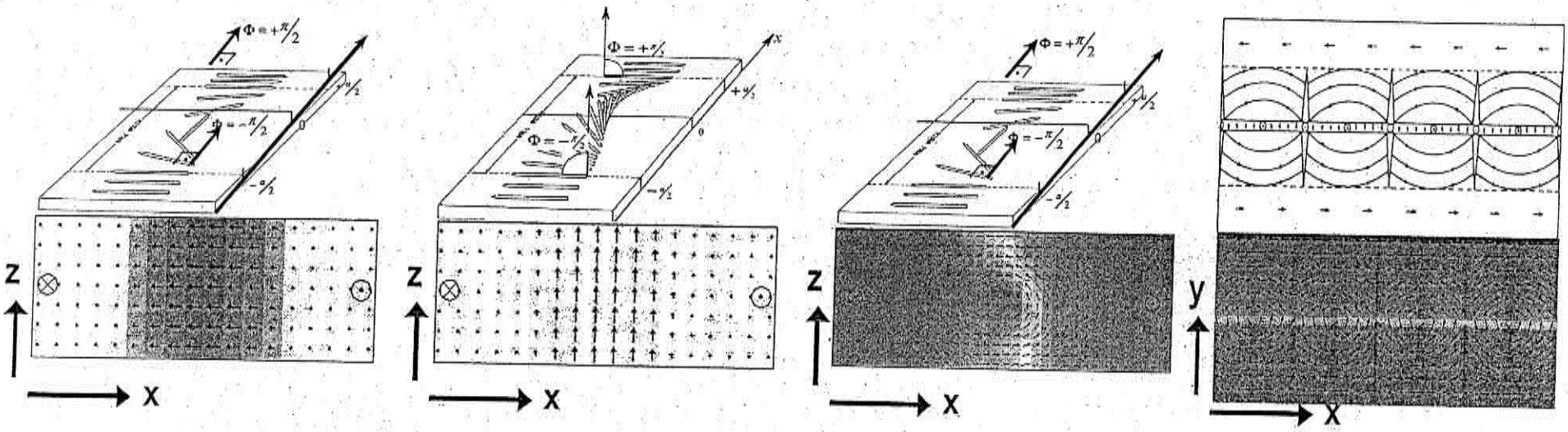

Néel-Wand

Bloch-Wand

Asymmetrische Bloch-Wand

Crosstie-Wand

Ferromagnetische Domänen

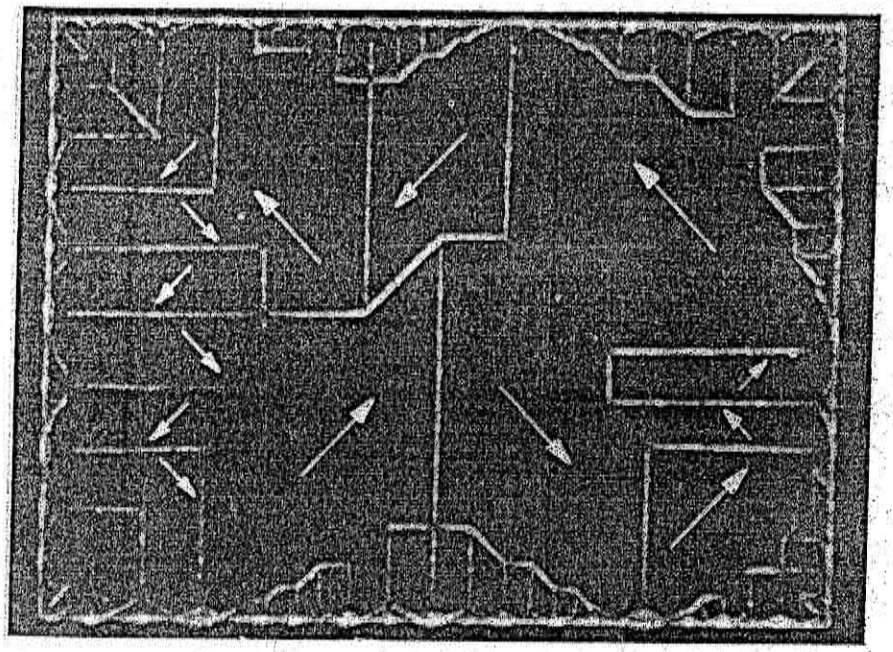

Wandbreite und –ausrichtung bestimmt durch Anisotropie

$$L_w = \sqrt{A/K}$$

Domänengröße bestimmt durch Wechselspiel zwischen Magnetostatischer und Austausch-Energie

$$L_{ex} = \sqrt{A/K_d}$$

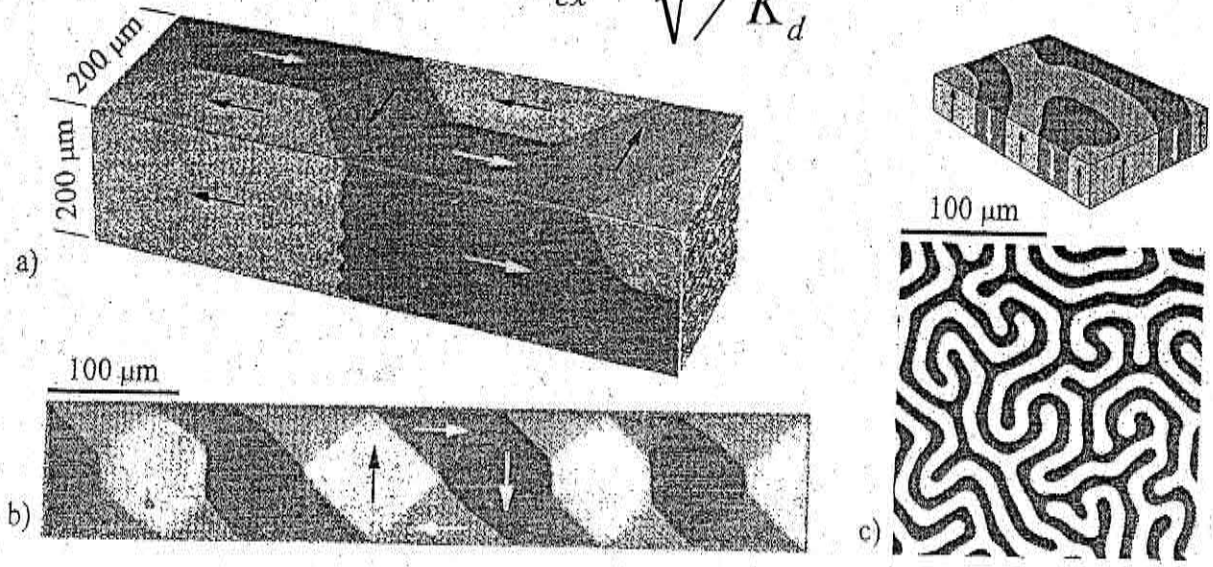

Modell-Hierarchie für ferromagnetische Materialien

Stoner-Wohlfarth-Modell

5. Magnetic Hysteresis, or Magnetization Curve
Describing the *average magnetization* vector of a sample
as a function of the external field (always applicable)

4. Phase, or Magnetic Texture Analysis
Collecting domains of equal magnetization direction in "phases". More generally,
describing the distribution function (*texture*) of magnetization directions (> 0.1 mm)

3. Domain, or Magnetic Microstructure Analysis
Describing the *magnetic microstructure* of a sample, the shape and detailed
spatial arrangement of domains and domain boundaries (1–1000 μm)

Mikromagnetisches Modell

2. Micromagnetic Analysis
g the *internal structure of domain walls* and their substructures in terms
ntinuum theory of a classical magnetization vector field (1–1000 nm)

1. Atomic Level Theory
Describing the origin, the interactions, the mutual arrangement
and the statistical thermodynamics of elementary magnetic moments (< 1 nm)

The values in parenthesis indicate the sample dimensions for which the different concepts are applicable

Stoner-Wohlfarth-Modell

E.C. Stoner and E.P. Wohlfarth, Phil. Trans. Roy. Soc. A-240, 599 (1948)

- Analytisches Modell, um die Hysterese eines Eindomänenteilchens mit uniaxialer Anisotropie zu berechnen.
- Wichtig für Vorhersagen über das Schaltverhalten von magnetischen Strukturen, z.B. Körner auf der Festplattenoberfläche

Geometrie

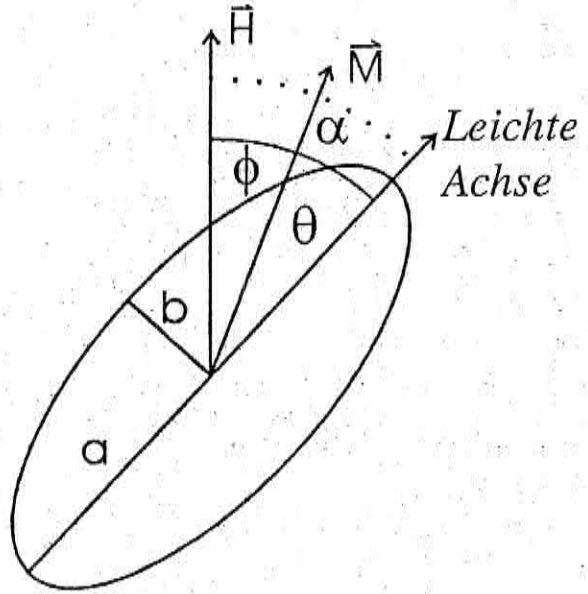

$$E_{Aniso} = K_1 \cdot V \cdot \sin^2 \theta$$

Berechnete Hystereseschleifen

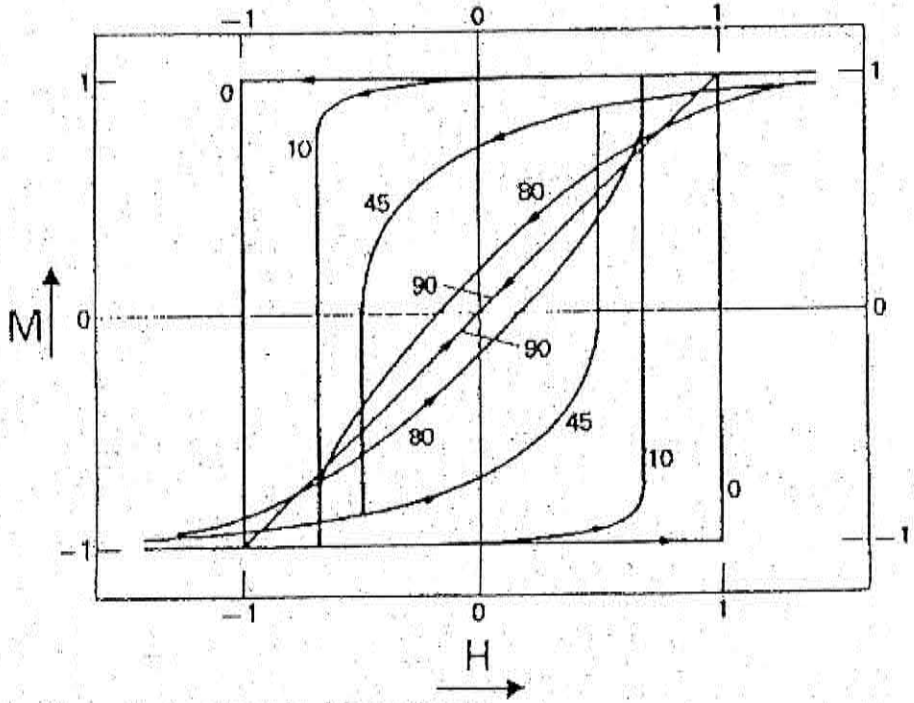

K ... Anisotropie Konstante

θ ... Winkel zwischen M und leichter Magnetisierungsrichtung

Stoner-Wohlfarth-Modell

E.C. Stoner and E.P. Wohlfarth, Phil. Trans. Roy. Soc. A-240, 599 (1948)

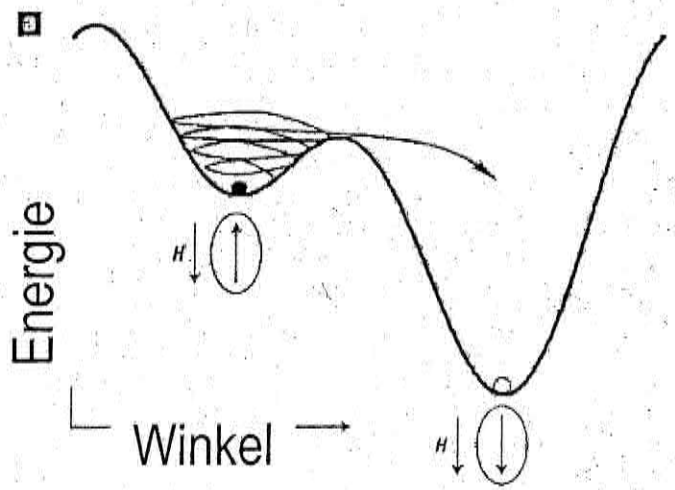

C. Thirion, Nature Mat. **2**, 524–527 (2003)

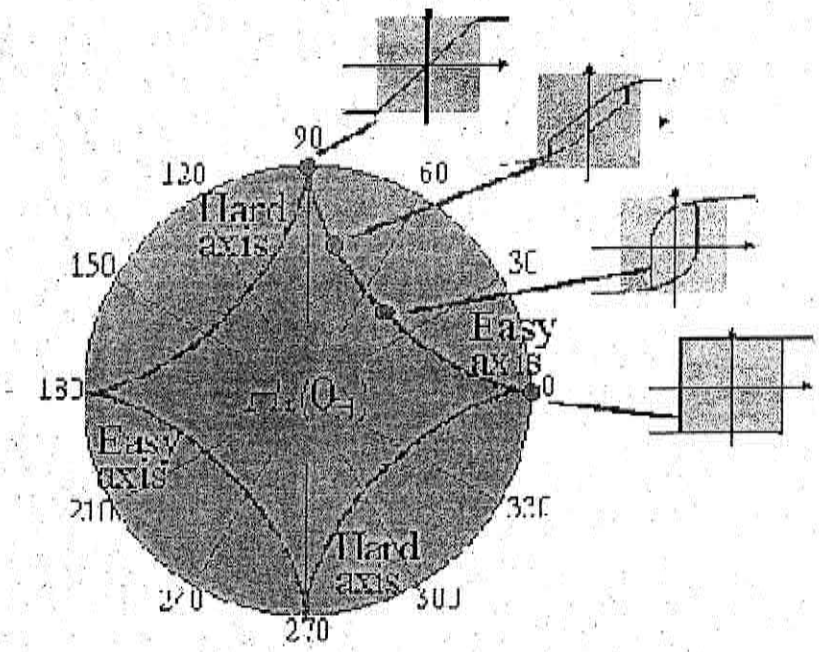

Quelle: CNRS Grenoble, France

a) Energie eines Eindomänenteilchens als Funktion des Winkels zwischen Magnetfeld und leichter Achse. Ist das Feld groß genug, so fällt das System in den energetisch günstigeren Zustand ins globale Energieminimum.

b) Aufgetragen die Umschaltfelder (schwarze Linien), bei denen ein Eindomänenteilchen den stabilen Zustand verläßt und instabil wird, also umschaltet. Die Form des Graphen nennt man auch Stoner-Wohlfarth-Astroid.

Coherent Rotation

With this chapter, we start to apply the concepts and the results developed so far to the description of the magnetization process and the prediction of magnetization curves in magnetic materials. According to the considerations made in chapters 6 and 7, the magnetization process is the result of complex and intricate rearrangements that involve a large number of degrees of freedom, in principle the whole vector field $\mathbf{M}(\mathbf{r})$ characterizing the magnetization state of the body. The description cannot be pushed very far if one insists in treating the problem with the maximum generality. In this chapter, we discuss what one can learn about magnetization processes, starting from the assumption that it is possible to identify elementary contributions, called "particles," which reverse their magnetization by coherent rotation, and that the overall behavior of the system is just the superposition of many of these contributions, which we suppose to act independently of each other. This program is inevitably associated with the names of Stoner and Wohlfarth, who in 1948 indicated the lines along which most of the subsequent studies have progressed. The approach is somewhat idealized and should not be expected to give accurate predictions of the behavior of real systems. However, it has an important pedagogical value, because it shows how certain physical concepts work in their simplest form and provides a sound basis for a number of generalizations.

The basic idea under *coherent rotation* is that a single magnetization vector is sufficient to describe the state of the whole system. We do not have any space dependence involved, and when the magnetization rotates under the action of the external field, the change is spatially uniform. The most natural example is that of a *magnetic particle* small enough to be a single domain (see Section 6.1.3). We shall see in Chapter 11 that coherent rotation is not the only mechanism by which magnetization reversal may take place. Yet coherent rotation is the case where we can calculate in a relatively simple way a lot of details about instability fields, dissipated

energy, and so on. In this respect, the concept of *astroid*, discussed in Section 8.1, plays a fundamental role and leads to the most elegant graphical representations of the stability properties of a single particle. After that, in Section 8.2 we discuss what kind of hysteresis phenomena arise from this description, and finally, in Section 8.3, we consider the overall behavior obtained by summing up many independent contributions. This can be the case in assemblies of weakly interacting magnetic particles or in the low-field response of bulk systems with random distributions of local anisotropy.

Although we shall constantly refer to "particles," we point out that the methods we are going to discuss have a wider applicability, because they do not require the existence of real particles under all circumstances. For example, a thin film or a certain portion of a continuous bulk system can also be studied by the same approach, as long as the assumption of uniform magnetization may be justified.

8.1 SINGLE PARTICLES

Imagine a small magnetic particle, of the type considered in Section 6.1.3. The particle has no domains. It is always saturated in a certain direction, so that we can describe its state by giving the orientation of its magnetization vector $\mathbf{M}$, or, equivalently, of the unit vector $\mathbf{m} = \mathbf{M}/M_s$. The particle may exhibit anisotropy, consequent to magnetocrystalline effects or to shape anisotropy (see Section 5.3). We consider the particular case of a spheroidal particle made up of a material with uniaxial magnetocrystalline anisotropy, and we assume that the crystal anisotropy axis coincides with the symmetry axis of the spheroid. According to Eq. (5.32) and Eq. (5.55), the magnetocrystalline and shape anisotropy energies have the same dependence on $\mathbf{m}$ orientation and can be summed up to give a total anisotropy energy density of the form

$$f_K(\mathbf{m}) = K \sin^2\theta \tag{8.1}$$

where θ is the angle between $\mathbf{m}$ and the anisotropy axis, and the effective anisotropy constant K is equal to

$$K = K_1 + K_M = K_1 + \frac{\mu_0 M_s^2}{2}\left(N_\perp - N_\parallel\right) \tag{8.2}$$

K_1 is the magnetocrystalline anisotropy constant, and Eq. (5.56) has been used for the shape anisotropy constant K_M. Equation (8.2) may be useful to connect the mathematical analysis to a well-defined physical situation, but it is not a necessary prerequisite. The results we shall obtain apply to whatever system, particle or not, for which the resulting anisotropy is uniaxial, and may be described by Eq. (8.1). The details of the mechanism responsible for the anisotropy will never come directly into play.

In this section, we discuss the behavior of a system of this sort when the external field $\mathbf{H}_a$ is varied in time. We shall always assume that the field variations are slow enough to avoid any dynamic effect. At the same time, we shall neglect the influence of temperature. We are thus in the limit of purely rate-independent hysteresis, in the sense discussed in Chapter 2. Thermal effects can be treated in terms of thermally activated jumps over energy barriers, a point that will be reconsidered in chapters 10 and 11.

8.1.1 The astroid

The behavior of the particle is governed by two energy terms, the uniaxial anisotropy energy described by Eq. (8.1) and the energy of interaction with the external field, $-\mu_0 M_s \mathbf{m}\cdot\mathbf{H}_a$. We assume that $K > 0$, which means that the anisotropy axis is an easy magnetization direction. Under zero field, $\mathbf{m}$ is aligned to the easy axis. When we apply the external field $\mathbf{H}_a$, $\mathbf{m}$ rotates away from the easy axis, toward the field, by an angle depending on the relative strength of anisotropy and field. Because of symmetry reasons, $\mathbf{m}$ will certainly lie in the plane containing the anisotropy axis and the external field. The problem is thus reduced to a two-dimensional problem in this plane. We call θ and θ_H the angles made by $\mathbf{m}$ and $\mathbf{H}_a$ with the easy axis (see Fig. 8.1), of which we conventionally choose one

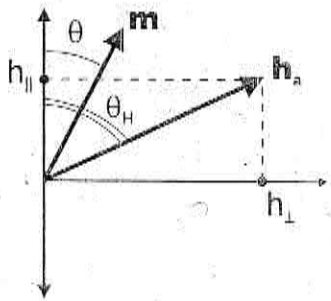

FIGURE 8.1. Relations between uniaxial anisotropy axis, magnetization unit vector, $\mathbf{m}$, and external field, $\mathbf{h}_a$.

orientation as the positive one. θ and θ_H vary in th[illegible]erval $(-\pi, \pi)$, with the convention that a positive (negative) angle means that the component of $\mathbf{m}$ or $\mathbf{H}_a$ perpendicular to the easy axis is positive (negative). The free energy of the particle is then

$$G_L(\theta;\mathbf{H}_a) = V[K \sin^2\theta - \mu_0 M_s H_a \cos(\theta - \theta_H)] \tag{8.3}$$

where V is the particle volume. The system is described by one state variable, the angle θ, and two control parameters, H_a and θ_H. It is convenient to write Eq. (8.3) in dimensionless form, by introducing the dimensionless quantities

$$g_L = \frac{G_L}{2KV} \qquad \mathbf{h}_a = \frac{\mu_0 M_s}{2K}\mathbf{H}_a = \frac{\mathbf{H}_a}{H_{AN}} \tag{8.4}$$

where H_{AN} is the anisotropy field.[1] We obtain

$$g_L(\theta;\mathbf{h}_a) = \frac{1}{2}\sin^2\theta - h_a \cos(\theta - \theta_H) \tag{8.5}$$

Instead of (h_a, θ_H) we shall use, when convenient, the field components perpendicular and parallel to the easy axis,

$$\begin{aligned} h_\perp &= h_a \sin\theta_H \\ h_\parallel &= h_a \cos\theta_H \end{aligned} \tag{8.6}$$

In terms of these variables, Eq. (8.5) becomes

$$g_L(\theta;\mathbf{h}_a) = \frac{1}{2}\sin^2\theta - h_\perp \sin\theta - h_\parallel \cos\theta \tag{8.7}$$

The magnetization process is governed by the stability properties of the system under varying external field. According to the general ideas discussed in Section 2.2.2, we should look at the qualitative changes in g_L when we move around in the control space represented by the plane of coordinates $h_\perp$ and $h_\parallel$. In this respect, a general conclusion can immediately be reached. Under zero field, there exist two energy minima, corresponding to $\mathbf{m}$ pointing up or down along the easy axis. For small fields around zero, we thus expect two states, one stable and one metastable, to be available to the system. Conversely, when $\mathbf{h}_a$ is very large, the energy of interaction with the field dominates and only one stable state is available, in which $\mathbf{m}$ is closely aligned to the field. Therefore, there must exist a closed curve around the origin separating the two-energy-minima low-field region from the one-energy-minimum outer plane. This contour represents the bifurcation set for our problem, that is, the set where Barkhausen jumps and discontinuous changes in the state of the system may take place. This curve turns out to be the *astroid* shown in Fig. 8.2.

To understand how we can arrive at this conclusion, let us consider that the bifurcation set is characterized by the fact that both the first and second derivative of g_L with respect to θ vanish. In fact, this is the condition indicating that one minimum and one maximum are merging and disappearing, giving rise to a horizontal inflection point. By calculating $\partial g_L/\partial\theta$ from Eq. (8.7) and by imposing the condition $\partial g_L/\partial\theta = 0$ one obtains the equation

$$\frac{h_\perp}{\sin\theta} - \frac{h_\parallel}{\cos\theta} = 1 \tag{8.8}$$

By calculating $\partial^2 g_L/\partial\theta^2$ and by imposing that $\partial^2 g_L/\partial\theta^2 = 0$ in addition to $\partial g_L/\partial\theta = 0$, one further obtains

$$\frac{h_\perp}{\sin^3\theta} + \frac{h_\parallel}{\cos^3\theta} = 0 \tag{8.9}$$

By eliminating in turn $h_\perp$ and $h_\parallel$ from Eq. (8.8) and Eq. (8.9), we arrive at the following parametric representation of the bifurcation set:

$$\begin{aligned} h_\perp &= \sin^3\theta \\ h_\parallel &= -\cos^3\theta \end{aligned} \tag{8.10}$$

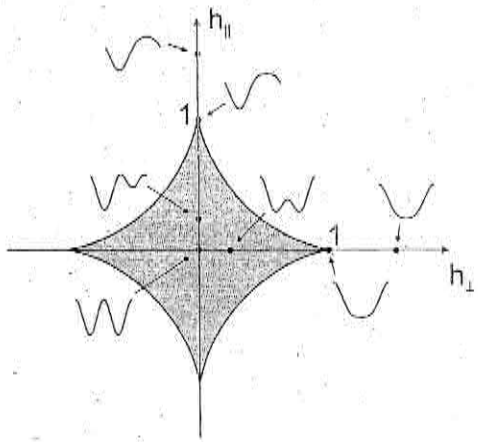

FIGURE 8.2. Control plane of coordinates $h_\parallel$ and $h_\perp$. The shaded region is delimited by the astroid curve defined by Eq. (8.10). Examples of the dependence of the system energy g_L (Eq. 8.7) on θ at different points in control space are shown.

[1]Note that this normalization is different from the one employed in Chapter 6 (Eq. 6.13).

where θ represents the orientation of $\mathbf{m}$ in the state losing stability at the point considered. The curve generated by Eq. (8.10) when θ varies in the interval $(-\pi, \pi)$ is the astroid shown in Fig. 8.2. By eliminating θ, Eq. (8.10) can also be written in the equivalent form

$$h_{\perp}^{2/3} + h_{\parallel}^{2/3} = 1 \tag{8.11}$$

Another representation is obtained by using polar coordinates, as in Eq. (8.6), and by expressing Eq. (8.11) in terms of h_a and θ_H:

$$h_a = \frac{1}{[\sin^{2/3}\theta_H + \cos^{2/3}\theta_H]^{3/2}} \tag{8.12}$$

Figure 8.2 contains pictures of the typical behavior of g_L as a function of θ at various points in control space inside and outside the astroid. g_L is a function of an angle coordinate, that is, a function on the circle, which exhibits either two minima and two maxima or one minimum and one maximum. The line $h_{\parallel} = 0$ coincides with the *Maxwell set*, in the sense of catastrophe theory (see Section 2.2.2 and Section 2.2.3). On the other hand, when one crosses the astroid curve along the $h_{\perp}$ axis, the *cusp catastrophe* is produced. This fact has interesting physical consequences, discussed in Section 8.3.3.

2.4 Der magneto-optische Kerr–Effekt

Die magnetischen Eigenschaften des Systems Kobalt auf Gold(111) werden mit Hilfe des magneto–optischen Kerr–Effekts untersucht. Um ein prinzipielles Verständnis des Effekts zu erhalten, werden zunächst eine kurze phänomenologische Erklärung und die zur Beschreibung nötigen Formeln gegeben. Abschließend werden die theoretisch zu erwartenden Kerr–Signale für das System Kobalt auf Gold (111) bestimmt.

2.4.1 Phänomenologische Beschreibung

Die Wechselwirkung von Licht mit einer magnetischen Probe führt zu dem magneto–optischen Kerr–Effekt. Die Analyse des reflektierten Lichts liefert Informationen über den magnetischen Zustand der Probe, welcher durch die Materialgleichungen beschrieben werden kann. Da im Frequenzbereich des Lichts, d. h. der elektromagnetischen Wellen, allgemein keine direkte Wechselwirkung des Magnetfelds der elektromagnetischen Welle mit der Magnetisierung der Probe zu erwarten ist, gilt für die Materialgleichung des Magnetfeldes[11] $\mathbf{B} = \mu_0 \mathbf{H}$ [7]. Die Materialgleichung der dielektrischen Verschiebung $\mathbf{D}$ der Wechselwirkung von Licht mit optisch isotropen Medien wird durch

$$\mathbf{D} = \epsilon_0 \epsilon_r (\mathbf{E} + i\mathbf{E} \times \mathbf{Q}) \tag{2.25}$$

beschrieben, wobei $\mathbf{E}$ das elektrische Feld, ϵ_r die relative Dielektrizitätskonstante und $\mathbf{Q}$ der Voigt–Vektor sind. Der Voigt–Vektor gibt die magnetischen Eigenschaften der Probe wieder und liegt bei optisch isotropen Medien parallel zur Magnetisierung [7]. Bei nicht vollständig transparenten Medien haben ϵ_r und $\mathbf{Q}$ einen Imaginärteil.

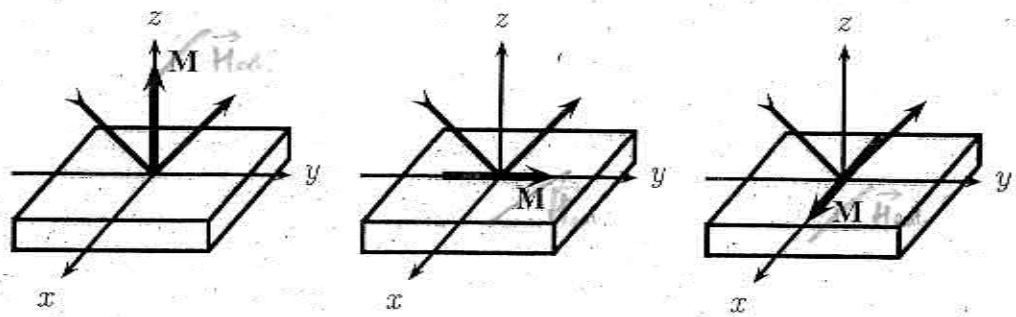

Abb. 2.12: Verschiedene MOKE–Geometrien

Zur Untersuchung der magnetischen Eigenschaften werden nach der Orientierung der Magnetisierung und der Einfallsebene des Lichts drei Kerr–Geometrien unterschieden: polare, longitudinale und transversale (vgl. Abb. 2.12). Bei der polaren Kerr–Geometrie liegt

[11] $\mathbf{B}$: Magnetfeld, $\mathbf{H}$: magnetische Feldstärke, μ_0: magnetische Feldkonstante des Vakuums. Für die relative magnetische Feldkonstante gilt $\mu_r = 1$.

die Magnetisierung in der Einfallsebene des Lichts und parallel zur Filmnormalen während sie in longitudinaler Geometrie in der Filmebene orientiert ist. In der transversalen Kerr–Geometrie liegt die Magnetisierung senkrecht zur Einfallsebene und parallel zur Filmebene.

Bei einer beliebigen Orientierung der Magnetisierung ergibt sich eine Überlagerung der magneto–optischen Beiträge aus den verschiedenen Geometrien. Umgekehrt ist für die Untersuchung der magnetischen Eigenschaften einer Probe die Kenntnis der zu erwartenden Beiträge zu dem Signal eine notwendige Voraussetzung. Die dafür nötigen Reflexions– und Transmissionskoeffizienten werden im folgenden Abschnitt vorgestellt.

2.4.2 Das Kerr–Signal ultradünner Filme

Die Reflexions– und Transmissionskoeffizienten werden durch Lösung der Maxwellschen Gleichungen mit den oben beschriebenen Materialgleichungen bestimmt [33–36]. Im Grenzfall ultradünner Filme ergibt sich eine analytische Lösung der Maxwellschen Gleichungen für die Reflexions– und Transmissionskoeffizienten unter der Voraussetzung, daß die optische Dicke der Probe deutlich geringer als die Wellenlänge des verwendeten Lichts λ ist, d. h. $n_m\, d_m \ll \lambda$ [33].[12] Die Reflexions– r und Transmissionskoeffizienten t gleicher Polarisationsrichtung sind unabhängig Beiträge von den optischen Eigenschaften des magnetischen Films.

$$r_{ss} = \frac{n_i \cos\theta_i - n_f \cos\theta_f}{n_i \cos\theta_i + n_f \cos\theta_f} \qquad t_{ss} = \frac{2n_i \cos\theta_i}{n_i \cos\theta_i + n_f \cos\theta_f}$$

$$r_{pp} = \frac{n_f \cos\theta_i - n_i \cos\theta_f}{n_f \cos\theta_i + n_i \cos\theta_f} \qquad t_{pp} = \frac{2n_f \cos\theta_i}{n_f \cos\theta_i + n_i \cos\theta_f}$$

Die Indizes s bzw. p der Koeffizienten kennzeichnen die Polarisationsrichtungen des einfallenden (zweiter Index) und des reflektierten Lichts. Bei s–Polarisation liegt die Polarisationsebene senkrecht zur Einfallsebene und bei p–Polarisation parallel. Mit dem Index wird i das Anfangsmedium (i. a. Vakuum) und mit f das Endmedium (für Co/Au(111): Gold) bezeichnet. n_i und n_f bezeichnen die Brechungsindizes. θ_i und θ_f sind der Einfalls– bzw. Austrittswinkel. Der Austrittswinkel θ_f wird über das Snellius'sche Brechungsgesetz bestimmt.

Durch den magnetischen Film ergibt sich eine Änderung der Lichtpolarisation, die durch

$$r_{ps} = r_{\text{pol}} - r_{\text{long}} \quad \text{und} \quad r_{sp} = r_{\text{pol}} + r_{\text{long}} \tag{2.26}$$

ausgedrückt werden kann. Die Reflexionskoeffizienten setzen sich additiv aus dem longitudinalen (Projektion der Magnetisierung auf die Filmebene, r_{long}) und dem polaren Beitrag (Projektion der Magnetisierung auf die Filmnormale, r_{pol}) zusammen[13] [37], die durch

$$r_{\text{pol}} = C_{\text{pol}} \cdot d_m Q \cos\alpha \quad \text{und} \quad r_{\text{long}} = C_{\text{long}} \cdot d_m Q \sin\alpha \tag{2.27}$$

[12] n_m: Brechungsindex des magnetischen Materials, d_m: Filmdicke.
[13] In der Dünnfilmnäherung ergibt sich kein transversaler Beitrag.

mit $C_{\text{pol}} = C \cdot \cos\theta_f n_m^2$, $C_{\text{long}} = C \cdot n_f n_i \sin\theta_i$ und $C = -\frac{\pi}{\lambda} \cdot \frac{t_{ss} t_{pp}}{n_i \cos\theta_i}$ beschrieben werden. Q_m ist die komplexe Voigt–Konstante des magnetischen Films und α der Winkel zwischen der Magnetisierung und der Filmnormalen. In Gleichung 2.27 wird weiterhin vorausgesetzt, daß sich die Magnetisierung in der Einfallsebene des Lichts befindet.

Der komplexe Kerr–Winkel Φ_K ist durch das Verhältnis der Reflexionskoeffizienten zueinander bestimmt:

$$\Phi_{Ks} = \theta_{Ks} + i\varepsilon_s := \frac{r_{ps}}{r_{ss}} \quad \text{bzw.} \quad \Phi_{Kp} = \theta_{Kp} + i\varepsilon_p := \frac{r_{sp}}{r_{pp}}. \tag{2.28}$$

Die Indizes s und p beziehen sich auf die oben eingeführten Polarisationsrichtungen. Zuvor linear polarisiertes Licht wird durch die Wechselwirkung zu elliptisch polarisiertem Licht. Die diese Änderung beschreibenden Größen sind die Rotation θ_K, d. h. der Winkel, um den die Polarisationsebene des Lichts durch die Wechselwirkung gedreht wird, und die Elliptizität ε, d. h. das Verhältnis der Hauptachsen der Ellipse (vgl. Abbildung 2.13). Elliptizität bzw. Rotation werden experimentell bestimmt.

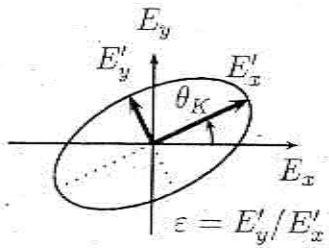

Abb. 2.13: Definition von Rotation θ_K und Elliptizität ε

Im Grenzfall ultradünner Filme ergibt sich eine lineare Abhängigkeit des Kerr–Signals, d. h. der Elliptizität oder der Rotation, von der Filmdicke (vgl. Gleichung 2.27). Während C_{long} durch den Faktor $\sin\theta_i$ eine ungerade Funktion in Abhängigkeit von dem Einfallswinkel θ_i ist, sind in C_{pol} nur gerade Funktionen von θ_i und θ_f zu finden. Dies bewirkt, daß der polare Beitrag unabhängig vom Einfallswinkel immer dasselbe Vorzeichen besitzt, während der longitudinale Beitrag sein Vorzeichen ändert. Dieser Unterschied kann experimentell zur Bestimmung der polaren und longitudinalen Beiträge ausgenutzt werden, vgl. Abschnitt 6.1.3.4 sowie Ding et al. [38].

Die Kerr–Signale können nicht nur in polare und longitudinale Beiträge sondern auch in von der Orientierung der Magnetisierung abhängige und unabhängige aufgeteilt werden. Die Kerr–Elliptizität wird zu

$$\varepsilon(\theta_i, \alpha) = \underbrace{\varepsilon_{\text{pol}}(\theta_i) m_\perp(\alpha)}_{\text{rein polar}} + \underbrace{\varepsilon_{\text{long}}(\theta_i) m_=(\alpha)}_{\text{rein longitudinal}} \tag{2.29}$$

umgeformt, wobei θ_i weiterhin der Einfallswinkel des Lichts und α der Winkel zwischen Filmnormalen und Magnetisierung ist. Es gilt $m_\perp = M_\perp/M_s = \cos\alpha$ und $m_= = M_=/M_s = \sin\alpha$. Der maximale polare bzw. longitudinale Beitrag ist durch

$$\varepsilon_{\text{pol}} = \text{Im}\left(\frac{C_{\text{pol}}}{r_{ss}} \cdot d_m \cdot Q\right) \quad \text{bzw.} \quad \varepsilon_{\text{long}} = \text{Im}\left(\frac{C_{\text{long}}}{r_{ss}} \cdot d_m \cdot Q\right) \tag{2.30}$$

bestimmt. Mit den im weiteren Verlauf der Arbeit verwendeten Begriffen von einem rein polaren bzw. rein longitudinalen Signal ist der erste bzw. zweite Teil der Elliptizität in Gleichung 2.29 gemeint. Diese Signale werden im Idealfall in den in Abbildung 2.12 dargestellten Geometrien bestimmt. Für die Kerr–Rotation gilt Gleichung 2.29 analog.

Chapter 1

Energetics of a ferromagnet

1.1 Magnetic free energy

A ferromagnet can be described at different levels of complexity [29] as a function of the scale of the system. The macroscopic properties of the magnetic materials can be deduced by the analysis of the hysteresis loops [26]. The domain theory describes the magnetic structure at the scale of $1 - 10^3$ μm [39]. The theory of micromagnetism is the base to describe magnetic microstructures at a scale of $1 - 10^3$ nm [14]. The goal of micromagnetics is to find the magnetization $\mathbf{M}(\mathbf{r})$ as a function of the position $\mathbf{r}$ inside the sample, under the constrain of constant module, i.e., $\mid \mathbf{M}(\mathbf{r}) \mid$=const.

The total free energy is given by:

$$\mathcal{G}(\mathbf{M}; \mathbf{H}_a) = \int_V g_{tot}(\mathbf{M}(\mathbf{r}); \mathbf{H}_a) dV = \int_V (f_{ex} + f_{an} + f_{ms} + f_h) dV \qquad (1.1)$$

where $g_{tot}(\mathbf{M}(\mathbf{r}); \mathbf{H}_a)$ is the total energy density given by the sum of exchange, anisotropy, magnetostatic and external field energies and $\mathbf{H}_a$ is an applied external field. In the following we introduce the various energy terms involved in eq. (1.1).

1.1.1 Exchange energy

The exchange is the basic interaction in ferromagnetic materials. The origin of it is electrostatic, but the explanation involves quantum mechanics. In fact, two electrons with spin vector $\mathbf{S}_i$ and $\mathbf{S}_j$ can be parallel or anti-parallel; in the first case, as a consequence of the principle of exclusion of Pauli, the two electrons have separate orbits and thus a reduced Coulomb interaction. Therefore the configuration with parallel spins is the lowest in energy. This explains the tendency of the magnetic materials to be constituted of wide regions of uniform magnetization called magnetic domains. The exchange energy associated with spin $\mathbf{S}_i$ and $\mathbf{S}_j$ is given by:

$$f_{ij} = -2\mathcal{J}\mathbf{S}_i \cdot \mathbf{S}_j \qquad (1.2)$$

where J is the exchange integral; $J > 0$ for a ferromagnet, $J < 0$ for an antiferromagnet. If the sample consists of more than one magnetic domain, not all spins can be collinear. If the angle between neighbor spins is small it is possible to make a Taylor expansion of the exchange energy. In the continuum approximation we obtain [28]:

$$f_{ex}(\mathbf{m}(\mathbf{r})) = A((\nabla m_x)^2 + (\nabla m_y)^2 + (\nabla m_z)^2) \tag{1.3}$$

where $A = \frac{nJS^2}{a}$, called exchange stiffness constant, is a function of the number of atoms per unit cell n, the lattice constant a, and $\mathbf{m}(\mathbf{r}) = \mathbf{M}(\mathbf{r})/M_s$, with M_s the saturation magnetization. The exchange is a short range interaction, as deducible from the quantum mechanic formulation. In fact, the wave functions bounded to different electrons have to overlap significantly in order to contribute to the exchange integral J. Besides, the exchange energy is an isotropic quantity because it depends only on the angle between neighbor magnetic moments and not on their relative orientation, as clear from eq. (1.3). Higher order anisotropic contributions are usually neglected.

1.1.2 Anisotropy energy

In magnetic materials the magnetization is induced to lie along specific direction called easy axis. The spin-orbit interaction couples the electron spins, responsible for the magnetism, to the anisotropic orbitals in a crystalline structure. The ions of the crystal create an electric potential that couples the spins to the lattice. The anisotropy energy is proportional to the product $\mathbf{L}\cdot\mathbf{S}$ between the orbital momentum $\mathbf{L}$ and the spin momentum $\mathbf{S}$. Therefore, in absence of magnetic field, the energetic minimum is obtained for $\mathbf{S}$ parallel to $\mathbf{L}$. A higher order source of anisotropy can be the stress, either tensile or compressive, applied to a crystal lattice. The stress changes the distance between neighbor ions so that the electric potential, the electronic orbitals and finally the spin-orbit coupling are modified. Both the magnetocrystalline anisotropy and the stress induced anisotropy find their origin in the spin-orbit coupling.

Hexagonal crystals like cobalt exhibit a uniaxial magnetic anisotropy. In this case the anisotropy energy density is given by the expansion of $\sin^2\theta$ [28], where θ is the angle between the c-axis and the magnetization:

$$f_u(\mathbf{m}(\mathbf{r})) = k_0 + k_1\sin^2\theta + k_2\sin^4\theta + \dots \tag{1.4}$$

The anisotropy constants k_1 and k_2 depend on the temperature and can be obtained exprimentally. The general formula in terms of expansion of direction cosine of $\mathbf{m}$ was given by Akulov [31]. In a cubic crystal, called α_1, α_2 and α_3 the cosine directors, the energy density result:

$$f_c(\mathbf{m}(\mathbf{r})) = k_0 + k_1(\alpha_1^2\alpha_2^2 + \alpha_2^2\alpha_3^2 + \alpha_3^2\alpha_1^2) + k_2(\alpha_1^2\alpha_2^2\alpha_3^2) + \dots \tag{1.5}$$

Equations (1.4) and (1.5) are volume energy densities. At surface the breaking of symmetry generates an additional term of anisotropy [29] given by:

Anisotropie

Austauschwechselwirkung ist isotrop (gleichförmig) verteilt, aber…

- Verteilung der nächsten Nachbarn durch die Gitterstruktur und

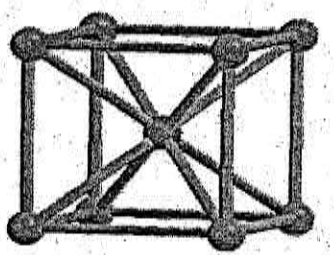

bcc-Gitter

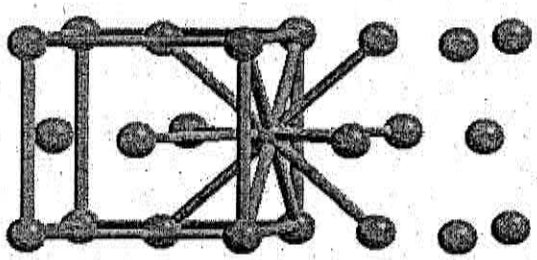

fcc-Gitter

- Elektronenorbitale sind es nicht.

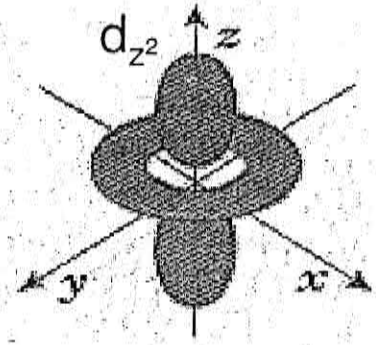

- Man unterscheidet **kubische** und **uniaxiale Anisotropie**, je nachdem, wie viele Symmetrieachsen ein Gitter hat (fcc, bcc haben drei Achsen, hexagonale eine).
- Anisotropiekonstante $\boldsymbol{K}$ als Maß für Ausrichtung in Symmetrie-Richtung.

$$f_s(\mathbf{m}(\mathbf{r})) = \frac{1}{2} k_s (\mathbf{n} \cdot \mathbf{m}(\mathbf{r}))^2 \tag{1.6}$$

where $\mathbf{n}$ is a unitary vector perpendicular to the surface and the constant k_s can be taken from the experiments. Note that equation (1.6), called surface anisotropy energy, can favors both an in-plane or an out-of-plane magnetization [32] and therefore the sign of k_s can be positive or negative.

1.1.3 External field energy

The interaction between the magnetization $\mathbf{M}(\mathbf{r})$ and an applied external field $\mathbf{H}_a$ results in the external field energy:

$$f_h(\mathbf{m}(\mathbf{r})) = -M_s \mathbf{H}_a \cdot \mathbf{m}(\mathbf{r}) \tag{1.7}$$

1.1.4 Magnetostatic energy

The magnetization $\mathbf{M}(\mathbf{r})$ can interact also with the magnetic field generated by the body itself. In this case the energy density is given by:

$$f_{ms}(\mathbf{m}(\mathbf{r})) = -\frac{1}{2} M_s \mathbf{H}_d \cdot \mathbf{m}(\mathbf{r}) \tag{1.8}$$

where the demagnetizing or stray field $\mathbf{H}_d$ is generated by the sample itself. The factor $\frac{1}{2}$ is introduced in order to avoid counting twice the interaction between couples of magnetic moments.

In order to calculate the magnetostatic energy we first need to evaluate $\mathbf{H}_d$. In this view we have to introduce some fundamental relations for magnetized media based on the equations of Maxwell. In absence of conduction currents the following relation is valid:

$$\nabla \times \mathbf{H}_d = 0 \tag{1.9}$$

In analogy with electrostatics, we can define the magnetic scalar potential ϕ that is linked to $\mathbf{H}_d$:

$$\mathbf{H}_d = -\nabla \phi \tag{1.10}$$

The magnetic potential ϕ is solution of Poisson's equation. Considering the boundaries at the surface of the ferromagnet we obtain

$$\phi(\mathbf{r}) = -\int_V \frac{\nabla \cdot \mathbf{M}(\mathbf{r}')}{|\mathbf{r} - \mathbf{r}'|} \, d^3r' + \oint_S \frac{\mathbf{n} \cdot \mathbf{M}(\mathbf{r}')}{|\mathbf{r} - \mathbf{r}'|} \, dS' \tag{1.11}$$

where the first is a volume integral over the body of volume V and the second is a surface integral extended to the surface S of the body. The form of equation (1.11) is analog to

the electrostatic potential. In fact, the first integral can be interpreted as the potential due to a spatial distribution of a volume charge with density $\rho = -\nabla \cdot \mathbf{M}$; the second as the potential due to a surface charge with density $\sigma = \mathbf{n} \cdot \mathbf{M}$.

In general, the calculation of the stray field $\mathbf{H}_d$ is complicated because it involves a three-fold integral, see eq. (1.11). In the case of a uniformly magnetized body $\nabla \cdot \mathbf{M} = 0$ and the first integral in eq. (1.11) vanishes. Moreover, M can be taken out of the surface integral and the potential depends only on the shape of the body. In particular, if the body is of ellipsoidal shape, the demagnetizing field $\mathbf{H}_d$ has the same direction as M:

$$\mathbf{H}_d = -4\pi \mathtt{D} \cdot \mathbf{M} \tag{1.12}$$

where D is a tensor. If M is parallel to one of the principal axis of the ellipsoid D is a number and it is called demagnetizing factor. The trace of the tensor D is 1. In a sphere for symmetry reasons the three demagnetizing factors are equal, $\mathtt{D}_x = \mathtt{D}_y = \mathtt{D}_z = \frac{1}{3}$. In an infinite cylinder along the z direction $\mathtt{D}_z = 0$ while $\mathtt{D}_x = \mathtt{D}_y = \frac{1}{2}$. In fact no surface charges are present at infinity, when the cylinder is magnetized along z. Similarly, a film infinitely extended in the xy plane has demagnetizing factors $\mathtt{D}_x = \mathtt{D}_y = 0$ and $\mathtt{D}_z = 1$. In all these cases it is easy to calculate the magnetostatic energy density from equations (1.12) and (1.8):

$$\mathtt{f}_{ms} = 2\pi(\mathtt{D}_x \mathtt{M}_x^2 + \mathtt{D}_y \mathtt{M}_y^2 + \mathtt{D}_z \mathtt{M}_z^2) \tag{1.13}$$

where $\mathtt{M}_i$ are the projections of the magnetization along the reference axis. In particular in the case of the infinite film eq. (1.13) becomes:

$$\mathtt{f}_{ms} = 2\pi \mathtt{M}_z^2 = 2\pi \mathtt{M}_s^2 \cos^2\theta \tag{1.14}$$

where θ is the angle of the magnetization vector with respect to the axis z. Equation (1.14) is characteristic of systems with uniaxial anisotropy (see eq. (1.4)) and is called shape anisotropy, because it depends only on the shape of the body. In fact, equation (1.14) may be generalized to the case of spheroid with $\mathtt{D}_x = \mathtt{D}_y \neq 0$. In the next chapters we will make wide use of eq. (1.14) in order to study thin films with uniform and non-uniform uniaxial anisotropy. The minimum of equation (1.14) is obtained for $\theta = 90°$, i.e., when the magnetization lies in-plane of the film. The direction of the easy axis is determined from the competition between shape and crystalline anisotropy.

Note that if the shape of the body is not ellipsoidal $\mathbf{H}_d$ is generally not uniform even if M is. In this case, equation (1.12) is no more valid.

1.2 Micromagnetic equations

The theory of micromagnetism developed in the 30ties with a study on the structure of magnetic walls between two antiparallel domains due to Landau and Lifshitz [27]. In the early 40ties W. F. Brown made fundamental steps to set the theory that he named

micromagnetics [14]. The theory considers in detail the magnetic microstructures that were neglected in domain theory [39]. The atomic nature of matter is ignored and the material is considered as continuous, i.e., the magnetization vector is taken as a continuous function of space.

In section 1 we introduced the energy terms useful to study the magnetization of a ferromagnet. In order to find the magnetization distribution we have to minimize the total energy of the system:

$$\mathtt{G}(\mathbf{M};\mathbf{H}_a) = \int_V (\mathtt{f}_{ex}(\mathbf{m}(\mathbf{r})) + \mathtt{f}_{an}(\mathbf{m}(\mathbf{r})) + \mathtt{f}_h(\mathbf{m}(\mathbf{r})) + \mathtt{f}_{ms}(\mathbf{m}(\mathbf{r}))\ \mathrm{d}^3\mathbf{r} + \int_S \mathtt{f}_s(\mathbf{m}(\mathbf{r}))\ \mathrm{d}S \tag{1.15}$$

where $\mathtt{f}$ are the energy densities. The set of local minima is found by means of variational calculus. The vector $\mathbf{m}(\mathbf{r})$ is varied in each point of the sample of a small quantity $\delta\mathbf{m}(\mathbf{r})$. The corresponding variation of the energy has to be zero, i. e. δG. In particular, the extreme is a minimum if the second-order variation of $\mathtt{G}$ is positive, i.e., $\delta^2\mathtt{G} \geq 0$. Following this scheme we will find the magnetization distribution for systems with spatially varying magnetic anisotropies, in chapter 4.

The solution of the variational problem takes the form of a stability condition to be fulfilled at equilibrium [26]. In each point of the magnetic body is defined an effective field $\mathbf{H}_{eff}$ given by:

$$\mathbf{H}_{eff} = -\frac{\partial \mathtt{G}(\mathbf{M};\mathbf{H}_a)}{\partial \mathbf{M}} \tag{1.16}$$

The effective field creates a torque on the magnetization that must be zero at equilibrium. Therefore the stability condition to be fulfilled in each point of the magnetic body is:

$$\mathbf{m} \times \mathbf{H}_{eff} = 0 \tag{1.17}$$

Equation (1.17) is known as equation of Brown and it is completed by the boundary conditions:

$$\mathrm{m} \times \left(2\mathtt{A}\frac{\partial \mathbf{m}}{\partial \mathrm{n}} + \frac{\partial \mathtt{f}_s}{\partial \mathbf{m}} \right) \tag{1.18}$$

where $\mathbf{n}$ is the unity vector normal to the surface and $\mathtt{A}$ is the exchange stiffness constant. In absence of surface anisotropy equation (1.18) becomes:

$$\frac{\partial \mathbf{m}}{\partial \mathrm{n}} = 0 \tag{1.19}$$

where the condition $\mathbf{m} \cdot \partial\mathbf{m}/\partial\mathrm{n} = 0$, valid for any vector of constant magnitude, has been used.

If the system is not in equilibrium equation (1.17) is not fulfilled and the vector $\mathbf{m}$ precess around the field $\mathbf{H}_{eff}$. From the experiments is known that the precession decays in a finite time [27]. As a consequence the temporal variation of $\mathbf{m}$ can be written as

$$\frac{\partial \mathbf{m}}{\partial t} = \gamma_G \mathbf{m} \times \left(\mathbf{H}_{eff} - \alpha_G \frac{\partial \mathbf{m}}{\partial t} \right) \tag{1.20}$$

where α_G is a phenomenological damping parameter and γ_G is proportional to the Lande' factor γ, i.e., $\gamma_G = \mu_0 \gamma$. Equation (1.20), called Gilbert's equation, is the generalization of eq. (1.17) to the dynamical case. If $\alpha_G \to 0$ the damping vanishes and the precession continues for ever. If $\alpha_G \to \infty$ the precession is negligible compared with the damping term. Finally, if $\partial \mathbf{m}/\partial t = 0$ the equation (1.17) is recovered.

THEORY OF OPERATION

Micromagnetic structure, such as that present in surface domain walls, can be extracted with standard methods for the solution to the Landau-Lifshitz-Gilbert equation. Such methods have been given in the literature by Brown [1], LaBonte [1,2], Aharoni [3-9], Hubert [10,11], and Schabes [9,12]. The equilibrium magnetization configuration results from the minimization of the system's free energy. The energy of a ferromagnetic system is composed of 1) the mean field exchange energy E_{ex} between nearest neighbors characterized by the exchange coupling constant A (erg/cm); 2) the magnetocrystalline anisotropy energy E_K, which describes the interaction of the magnetic moments with the crystal field characterized by the constant K_v (erg/cm^3); 3) the surface magnetocrystalline anisotropy energy E_{ks}, which corrects for broken symmetry near surfaces in the interaction of the magnetic moments with the crystal field, and is characterized by the constant K_s (erg/cm^2); 4) the magnetostatic self-energy E_s, which arises from the interaction of the magnetic moments with the magnetic fields created by discontinuous magnetization distributions both in the bulk and at the surface; 5) the external magnetostatic field energy E_h, which arises from the interaction of the magnetic moments with any externally applied magnetic fields; and 6) the magnetostrictive energy E_r, which arises when mechanical stress (strains) are applied to a ferromagnetic material thereby introducing effective anisotropy into the system characterized by K_m (erg/cm^3).

The solution for the equilibrium magnetization distribution is a constrained boundary value problem in two or three spatial dimensions with the constraint of constant magnetization M_s. The continuous magnetization distribution of a ferromagnet is approximated by a discrete magnetization distribution consisting of equal volume cubes (3-D) or rods (2-D). Each individual discretized magnetization cell, interior to the array, will be addressed by the (X, Y, Z) coordinates of its centroid. There are N_x cells along X, N_y cells along Y, and N_z cells along Z interior to the structure to be modeled.

There is one plane (3-D) or column (2-D) of boundary cells bounding the discretized region. These boundary cells (conditions) can reflect the continuous uniform magnetization distribution present within the domains themselves on either side of the structure. If no boundary conditions are specified, the cells at the edges are free. In the absence of surface anisotropy, the normal derivative of the magnetization distribution at the surface is zero [2,13]. In the presence of surface anisotropy, the Rado-Weertman boundary conditions is used [13,14].

Fundamental to the solution of the micromagnetic equations is the assumption that the bulk saturation magnetization M_s (emu/cm^3) is constant microscopically throughout the ferromagnet. The parameter M_s represents saturation magnetization at room temperature. For most practical systems being considered (Fe, Co or Permalloy), there is little deviation in M_s at room temperature from the 0 K value. The value of the magnetization vector $\mathbf{M}(\mathbf{r})$ at each point within the ferromagnet is the saturation magnetization multiplied by the direction cosines, that is $\mathbf{M}(\mathbf{r}) = (M_x(\mathbf{r}), M_y(\mathbf{r}), M_z(\mathbf{r})) = M_s\alpha(\mathbf{r}) = M_s(\alpha(\mathbf{r}), \beta(\mathbf{r}), \gamma(\mathbf{r}))$. The constraint equation implied by the constant magnetization assumption is $|\alpha(\mathbf{r})| = 1$. The individual contributions to the energies in this continuum model are calculated by integrating the energy expressions over the structure in question. The energy integrals below are integrated over the appropriate dimension, dV. The exchange energy E_{ex} in the continuum approximation is given by.

$$E_{ex} = \int dV[|\nabla\alpha|^2 + |\nabla\beta|^2 + |\nabla\gamma|^2]$$

The exchange parameter A can be extracted from spin-wave theory [15-17], which shows that $A = A'M_s^2 = DS/2V$, where D is the spin-wave dispersion parameter, S is the spin per atom and V is the volume per atom. The spin-wave dispersion parameter, D, is related to the exchange constant, J, in the Heisenberg hamiltonian by $D = 2JSa2$, where 'a'

is the lattice spacing. This relationship is true for spin-wave modes along bcc [100], bcc [110], fcc [110] and fcc [100] directions.

The volume magnetocrystalline anisotropy for uniaxial (e.g. easy-axis in y) E_{Ku}, and cubic crystals E_{Kc}, is given by the following expressions, respectively,

$$E_{Ku} = \int dV\left[K_{u1}(1-\beta^2) + K_{u2}(1-\beta^2)^2\right]$$

$$E_{Kc} = \int dV\left[K_{c1}\left(\alpha^2\beta^2 + \beta^2\gamma^2 + \alpha^2\gamma^2\right) + K_{c2}\alpha^2\beta^2\gamma^2\right]$$

where the bulk anisotropy constants for cubic, Kc, and uniaxial, Ku, symmetry can be determined from torque magnetometry measurements. The energy due to magnetostriction can be included in the expression for the uniaxial anisotropy by appropriately adjusting the value of the anisotropy constant [20]. The surface magnetocrystalline anisotropy energy E_{Ks} is given by,

$$E_{Ks} = \int dS \frac{1}{2}(\hat{\alpha} \bullet \hat{n})^2$$

where the integration is along the (line increment dS in 2-D or a surface increment in 3-D) boundary at the film surfaces. The symmetry of the surface anisotropy energy was determined by Rado [21,22].The self-magnetostatic field energy E_s can be represented in a number of equivalent forms, but for these purposes the most convenient representation is

$$E_s = -\int dV \frac{1}{2}\vec{H}_s \bullet \hat{\alpha} M_s$$

where the self-field $\mathbf{H}_s$ is determined from the negative gradient of the scalar magnetic potential,

$$\vec{H} = -\nabla \phi$$

The magnetic scaler potential ϕ satisfies

$$\nabla^2 \phi = 4\pi M_s \nabla \bullet \hat{\alpha}$$

inside the ferromagnet, and LaPlace's equation outside of the ferromagnet,

$$\nabla^2 \phi' = 0$$

and at the surface $\phi = \phi'$ and

$$-\frac{d\phi}{dz} + 4\pi M_s \gamma = -\frac{d\phi}{dz}$$

in the two-dimensional case for example. The regularity of ϕ' at infinity is also required. This can be guaranteed by solving for the potential using Green's function methods. The calculation of this self- field energy is the most computationally intensive aspect of solving the micromagnetic equations. The external field energy E_h for an applied field of $\mathbf{H}_o$ is simply given as

$$E_h = -\int dV \vec{H}_o \bullet \hat{\alpha} M_s$$

To calculate the magnetic microstructure in ferromagnets, the time evolution of a magnetization configuration inside ferromagnet, which is described by the Landau-Lifshitz-Gilbert equation, must be solved. The Landau-Lifshitz-Gilbe equation has been examined experimentally and theoretically [28,29,32,81,82], and found to yield an accurate desc tion of the time evolution of a magnetic moment of fixed magnitude in a magnetic field. This equation has the followi form.

$$d\vec{M}/dt = -\frac{\gamma}{1+\alpha^2}\vec{M}\times\vec{H}_{eff} - \frac{\gamma\alpha}{(1+\alpha^2)M_s}\vec{M}\times\vec{M}\times\vec{H}_{eff}$$

Here, the gyromagnetic frequency $\gamma = g\omega_e/2$ is determined from the free electron value of ω_e and the spectroscopic splitting factor, g = 2. The gyromagnetic frequency γ, the damping parameter α and the magnitude of the effective fiel determine the time scales of interest. For time domain simulations, the free electron gyromagnetic frequency of $\gamma = 1.7 \times 10^7$ (Oe sec-1) is used. The damping parameter α is not well known. Values of α between 0.005 and 2.0 have beer used to solve LLG. The damping parameter was not found to change the equilibrium magnetization configurations in domain walls in uniform ferromagnetic systems [23]. The effective magnetic field on each magnetic moment is determined from the total system energy E_{tot} as

$$\vec{H}_{eff} = -\partial E_{tot}/\partial(M_s\hat{\alpha})$$

The effective magnetic field incorporates all the effects of exchange, anisotropy, external fields and demagnetizing fields. For the analysis of the equilibrium micromagnetic structure, the differential equation need not be integrated directly. Instead, notice that, for an equilibrium magnetization distribution, dM/dt = 0, which implies that the effective field, $\mathbf{H}_{eff}$, must be parallel to the magnetization **M**. The magnetization configuration can be relaxed iteratively by positioning each magnetization vector (almost) along the effective field vector direction throughout the mesh. The initial condition can be selected to provide a head start for the iteration procedure. When the largest residual of a single value of $(\mathbf{M}\times\mathbf{H}_{eff})/|\mathbf{M}||\mathbf{H}_{eff}|$ decreases below a convergence minimum, the iteration process is stopped. The convergence minimum for terminating the calculation is the value of the largest relative change in the largest component of the direction cosines. This value will depend upon the size of the mesh and on the closeness to a magnetization change, such as the reorientation close to the coercive field in a hysteresis loop calculation. Equilibrium domain wall configurations determined from this energy minimization scheme agree extremely well with configurations determined by solving the Landau-Lifshitz-Gilbert equation directly [23]. For equilibrium configurations for uniform systems, the more economical energy minimization scheme can be used to determine equilibrium configurations. For more complex systems, or in the presence on grain boundaries, which may serve as nucleation sites, the solution of the Landau-Lifshitz-Gilbert equation is necessary for accurate results [18,19].

The content of this section has been extracted and slightly altered from the original version published in a section of Micromagnetics of 180 Degree Domain Walls at Surfaces, M.R. Scheinfein, J. Unguris, J.L. Blue, K.J. Coakley, D.T. Pierce, R.J. Celotta, P.J. Ryan, Phys. Rev. B43(4), 3395 (1991).

1. W.F. Brown, A.E. LaBonte, J. Appl. Phys. **36**(4), 1380 (1965).
2. A.E. LaBonte, J. Appl. Phys. **40**(6), 2450 (1969).
3. A. Aharoni, J. Appl. Phys. **37**(8), 3271 (1966).
4. A. Aharoni, J. Appl. Phys. **38**(8), 3196 (1967).
5. A. Aharoni, Phil. Mag. **26**, 1473 (1972).
6. A. Aharoni, phys. stat. sol. (a) **18**, 661 (1973).
7. A. Aharoni, J. Appl. Phys. **46**(2), 908 (1975).
8. A. Aharoni, J. Appl. Phys. **46**(2), 914 (1975).
9. M.E. Schabes, A. Aharoni, IEEE Trans. Mag. MAG-**23**(6), 3882 (1987).
10. A. Hubert, phys. stat. sol. **32**, 519 (1969).

11. A. Hubert, phys. stat. sol. **38**, 699 (1970).
12. M.E. Schabes, H.N. Bertram, J. Appl. Phys. **64**(3), 1347 (1988).
13. G.T. Rado, J.R. Weertman, J. Phys. Chem. Solids, **11**, 315 (1959).
14. G.T. Rado, Phys. Rev. **B40**(1), 407 (1989).
15. R. Victora, J. Appl. Phys. **62**(10), 4220 (1987).
16. C. Herring, C. Kittel, Phys. Rev. **81**(5), 869 (1951).
17. G. Shirane, V.J. Minkiewicz, R. Nathans, J. Appl. Phys. **39**(2), 383 (1968).
18. C.C. Shir, J. Appl. Phys. **49**(6), 3413 (1978).
19. R. Victora, Phys. Rev. Lett. **58**(17), 1788 (1987).
20. B.D. Cullity, Introduction To Magnetic Materials (Addison Wesley Publishing Co, Reading, 1972).
21. G.T. Rado, Phys. Rev. **B26**, 295 (1982).
22. G.A. Prinz, G.T. Rado, J.J. Krebs, J. Appl. Phys. **53**(3), 2087 (1982).
23. M.R. Scheinfein and J.L. Blue, J. Appl. Phys. **69**(11), 7740 (1991).

Verwendete Literatur

- G. Bertotti, Hysteresis in magnetism, Academic Press (1998)
- S. Pütter, *Dissertation,* Universität Halle-Wittenberg (2000), http://sundoc.bibliothek.uni-halle.de/diss-onlin
- F. Porrati, *Dissertation,* Universität Halle-Wittenberg (2002), http://sundoc.bibliothek.uni-halle.de/diss-online
- M. R. Scheinfein, LLG user manual v2.46 (2002)

Weitere Literatur

- E. Kneller, Ferromagnetismus, Springer-Verlag (1962)
  Max Born Bibliothek. Signatur: Fck 26
- A. Hubert, R. Schäfer, Magnetic domains, Springer-Verlag (1998)
  Max Born Bibliothek. Signatur: Fck 171
- H.-J. Elmers, "Magnetismus in dünnen Filme" in Magnetische Schichtsysteme IFF- Ferienkurse (1999). Max Born Bibliothek. Signatur: So 123/1999

Anwendungen Magnetische Materialien

Field of application	*Products*	*Requirements*	*Materials*
Power conversion electrical - mechanical	Motors Generators Electromagnets	Large M_R Small H_C Low losses = small conductivity low ω	Fe based materials, e.g. Fe + ≈ (0,7 - 5)% Si Fe + ≈ (35 - 50)% Co
Power adaption	(Power) Transformers		
Signal transfer	Transformer ("Überträger")	Linear M - H curve	Fe + ≈ 36 % Fe/Ni/Co ≈ 20/40/40
	LF ("low" frequency; up to ≈ 100 kHz)	Small conductivity medium ω	Ni - Zn ferrites
	HF ("high" frequency up to ≈ 100 kHz)	Very small conductivity high ω	
Magnetic field screening	**"Mu-metal"**	Large **dM/dH** for **H** ≈ 0 ideally $\mu_r = 0$	Ni/Fe/Cu/Cr ≈ 77/16/5/2
Permanent magnets	Loudspeaker Small generators Small motors Sensors	Large H_C (and M_R)	Fe/Co/Ni/Al/Cu ≈50/24/14/9/3 $SmCo_5$ $Sm_2Co_{17}Fe$ NdFeB ($Nd_2Fe_{14}B$)
Data storage analog	Video tape Audio tape	Medium H_C (and M_R), hystereses loop as rectangular as possible	NiCo, CuNiFe, CrO_2 Fe_2O_3
Data storage digital	Ferrite core memory Drum		
	Hard disc, Floppy disc		
	Bubble memory	Special domain structure	Magnetic garnets(AB_2O_4, or $A_3B_5O_{12}$), e.g. with A = Yttrium (or mixtures of rare earth), and B = mixtures of Sc, Ga, Al Most common: $Gd_3Ga_5O_{12}$
Quantum devices	**GMR** reading head	Special spin structures in multilayered materials	Permalloy
	MRAM		

M_R = remanence ; H_C = coercivity; ω = frequency

6. Die Anwendung des Kerr-Effekts: Magnetooptische Datenspeicherung

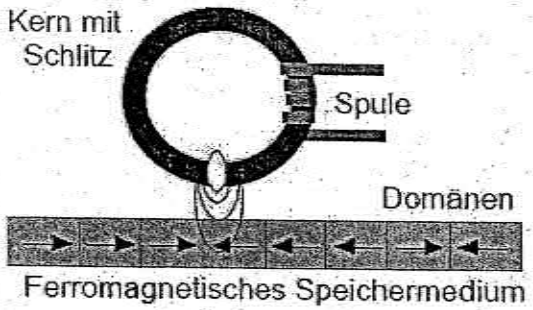

Abb. 18: Konventionelle Datenspeicherung mit in-plane-Magnetisierung

Bei magnetischen Datenspeichern der vorigen Generation, wie sie z.B. bei Diskettenlaufwerken verwendet werden, erfolgt das Lesen und Schreiben von Daten mit Hilfe eines von einer Spule generierten Magnetfelds (Abb. 18). Hierbei werden im Speichermedium longitudinal magnetisierte Domänen erzeugt. Zum Lesen der Domänenstruktur wird die bei der Bewegung über die Probenoberfläche in die Spule induzierte Spannung ausgewertet.
Die Versuche, die Daten auf dem Speichermedium immer weiter zu integrieren, stießen jedoch an technische Grenzen: Zum einen ist es unmöglich, die Spulen bzw. Kerne beliebig klein zu produzieren, um so immer kleinere Domänen schreiben zu können. Zum anderen erfordern die heute verwendeten Spurbreiten von ca. 10µm eine „Flughöhe" der Spule über dem Speichermedium, bei der der reguläre „berührungslose" Betrieb und der Totalschaden durch einen Headcrash nur noch wenige µm auseinander liegen.

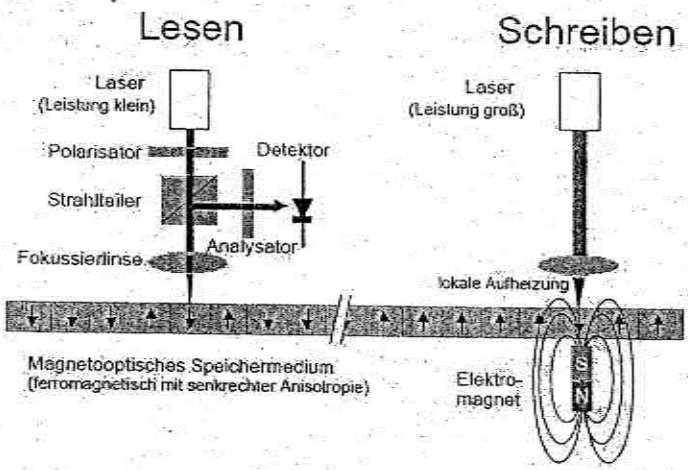

Abb. 19: Lesen und Schreiben eines magnetooptischen Datenspeichers mit out-of-plane-Anisotropie

Als Lösung bietet sich eine Abtastung des Datenspeichers durch einen (Laser-)Lichtstrahl an, der sich mit einem Linsensystem problemlos auf einige Mikrometer fokussieren lässt. Die

Daten auf einer CD werden durch eine eingepresste Spur von ca. 1x2 µm große Vertiefungen („Pits") gespeichert, an denen der Laserstrahl gestreut wird.
Die Magnetooptik bietet eine gelungene Symbiose aus einem einfach überschreibbaren magnetischen Speichermaterial und dem verschleißfreien Lesen und Schreiben mit dem Laserstrahl. Benutzt wird dazu der magnetooptische Kerr-Effekt. Das Lesen erfolgt durch Auswertung des Kerr-Winkels bei der Reflexion an der senkrecht zur Oberfläche magnetisierten Probe (Abb. 19).

Zum Schreiben von Informationen wird ein Laserstrahl höherer Intensität auf die Probe fokussiert, so dass das ferromagnetische Speichermedium lokal stark erwärmt wird. Weil beim Erwärmen die Koerzitivfeldstärke des Materials stark abfällt, lässt sich die Probe mit einem schwachen Feld eines externen Elektromagneten an der aufgeheizten Stelle beliebig ummagnetisieren, ohne dass die Umgebung dadurch beeinflusst wird. In Abbildung 20 ist schematisch die Temperaturabhängigkeit des Koerzitivfeldes eines Ferromagneten dargestellt. Bei Raumtemperatur soll H_C größer als das externe Ummagnetisierungsfeld H_S sein, wodurch die magnetischen Domänen stabil sind. Wird das Material über eine kritische Temperatur T_S aufgeheizt, wird $H_C<H_S$ und die Domänen können ummagnetisiert und somit Informationen geschrieben werden.

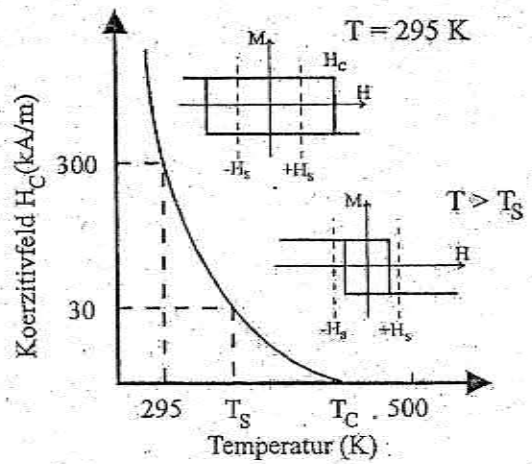

Abb. 20: Schematisch dargestellte Temperaturabhängigkeit des Koerzitivfelds bei lokaler Erwärmung
T_C: Curie-Temperatur, H_C: Koerzitivfeld, H_S: externes Ummagnetisierungsfeld, T_S: kritische Temperatur[1]

[1] P.Fumagalli: Skriptum „Magnetooptik, Grundlagen und ihre Anwendungen", Vorlesungen an der RWTH-Aachen, nicht verlegt, Abb. 63